

Inspecting class hierarchies in classification-based metric learning models

Hyeongji Kim^{1,2*}, Pekka Parviainen², Terje Berge¹, Ketil Malde^{1,2}

1 Institute of Marine Research, Bergen, Norway

2 Department of Informatics, University of Bergen, Norway

* hjk92g@gmail.com

Abstract

Most classification models treat all misclassifications equally. However, different classes may be related, and these hierarchical relationships must be considered in some classification problems. These problems can be addressed by using hierarchical information during training. Unfortunately, this information is not available for all datasets. Many classification-based metric learning methods use class representatives in embedding space to represent different classes. The relationships among the learned class representatives can then be used to estimate class hierarchical structures. If we have a predefined class hierarchy, the learned class representatives can be assessed to determine whether the metric learning model learned semantic distances that match our prior knowledge. In this work, we train a softmax classifier and three metric learning models with several training options on benchmark and real-world datasets. In addition to the standard classification accuracy, we evaluate the hierarchical inference performance by inspecting learned class representatives and the hierarchy-informed performance, i.e., the classification performance, and the metric learning performance by considering predefined hierarchical structures. Furthermore, we investigate how the considered measures are affected by various models and training options. When our proposed ProxyDR model is trained without using predefined hierarchical structures, the hierarchical inference performance is significantly better than that of the popular NormFace model. Additionally, our model enhances some hierarchy-informed performance measures under the same training options. We also found that convolutional neural networks (CNNs) with random weights correspond to the predefined hierarchies better than random chance.

Introduction

Neural network-based classifiers have shown impressive classification accuracy. For instance, a convolutional neural network (CNN) classifier [1] surpassed human-level top-5 classification accuracy (94.9%) [2] on the 1000-class classification challenge on the ImageNet dataset [3]. Most training loss functions in neural network classifiers treat all misclassifications equally. However, in practice, the severity of various misclassifications may differ considerably. For instance, in an autonomous vehicle system, mistaking a person as a tree can result in a more catastrophic consequence than mistaking a streetlight as a tree [4]. In addition, some classification tasks include a large number of classes, such as the 1000-class ImageNet classification challenge, and hierarchical relationships may exist among these classes. When several classification models

achieved similar accuracy, one would prefer to choose models in which the wrongly predicted classes are “hierarchically” close to the ground-truth classes. To address the severity of misclassifications and relationships among classes, hierarchical information can be used. For instance, predefined hierarchical structures can be incorporated into training by replacing standard labels with soft labels based on this hierarchical information [4]. Some metric learning approaches also use hierarchical information [5–7].

In general, metric learning methods learn embedding functions in which similar data points are close and dissimilar data points are far apart according to the distance metric in the learned embedding space. For class-labeled datasets, data points in the same class are regarded as similar, while data points in different classes are regarded as dissimilar. Metric learning can be applied in image retrieval tasks [8] to identify relevant images or few-shot classification tasks [9,10], which are classification tasks with only a few examples per class. Usually, metric learning methods assume that there are no special relations among classes, i.e., a flat hierarchy is assumed. However, a predefined class hierarchy can be incorporated into the training process of metric learning models to improve the hierarchy-informed performance [5–7].

Class hierarchical structures can be defined in several ways. Hierarchical structures can be defined by domain experts [6] or extracted from WordNet [11], which is a database that contains semantic relations among English words. For instance, ImageNet classes [3] are organized according to WordNet. However, hierarchy determination from WordNet requires that a class name or its higher class is in the WordNet database. When these approaches are not applicable, hierarchy can be inferred by estimating the class distance matrix based on learned classifiers. For instance, the confusion matrix of a classifier can be used to estimate relations among class pairs [12]. Each row in the confusion matrix can be treated as a vector, and the distance between these vectors can be calculated to estimate the class hierarchical structure. However, this approach can be cumbersome for hierarchy-informed classification tasks, as they require separate training and evaluation (validation) processes to determine the hierarchical structure. Moreover, this approach becomes challenging when some classes contain a very small number of data points, as some elements in the confusion matrix may be uninformative. One type of metric learning model uses a unique position in embedding space (class representative) to represent each class [13–16]. Class representatives can also be used to infer hierarchical structures by considering their distances [6,17]. This approach does not require a separate training process, as class representatives can be learned automatically.

On the other hand, when we have a predefined hierarchy, the learned class representatives can improve our understanding of the trained metric learning model. For example, we can determine if the semantic distance learned by a metric learning model matches our prior knowledge (that is, the predefined hierarchy). For instance, when a model has been trained to classify species, we can determine if the model regards a dog as closer to a cat than to a rose. Furthermore, these inspections can be used to evaluate the trustworthiness of a model. However, previous works have paid little attention to the relationships among class representatives. In this work, we assess several metric learning methods and training options by focusing on their learned class representatives and hierarchy-informed performance. Moreover, we attempt to determine conditions that improve the hierarchy inference performance and evaluate whether such models enhance the hierarchy-informed performance. We also investigate different training options with predefined hierarchies for comparison.

Problem settings

The predefined hierarchical distance, i.e., the distance between two classes, often needs to be considered when training models with hierarchical information and evaluating

model performance. Barz and Denzler [5] and Bertinetto et al. [4] used bounded $([0, 1])$ dissimilarity based on the height of the lowest common ancestor (LCA) between two classes. In this work, similar to Garnot and Landrieu [6], we define the hierarchical distance as the shortest path distance between two classes. For instance, in the predefined hierarchical tree shown in Fig. 1, the hierarchical distance between the classes “tiger” and “woman” is 4 ($= 2 + 2$), as we need to move two steps upward and two steps downward to move from one class to the other. Similarly, the hierarchical distance between the classes “tiger” and “shark” is 6. Hierarchical structures can be expressed as trees or directed acyclic graph (DAG) structures [18]. In this work, we consider tree-structured hierarchies. In other words, each node cannot have more than one parent node.

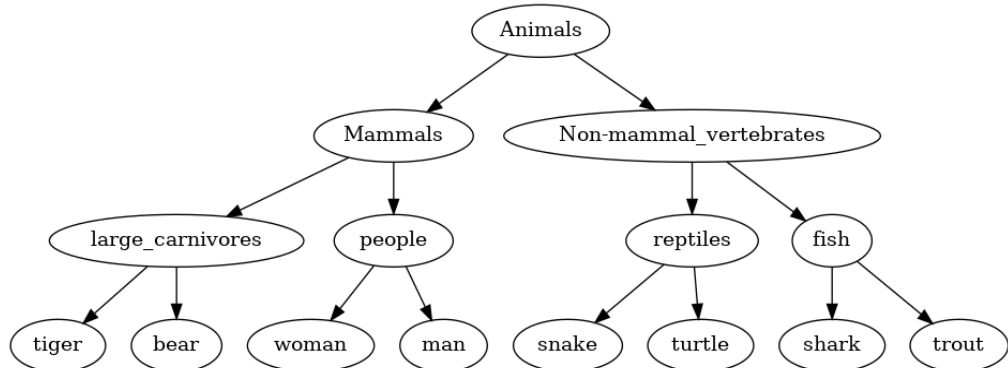


Fig 1. Pruned CIFAR100 tree structure for visualization. The whole hierarchical structure is shown in a table in S2 Appendix.

Let $\mathcal{X} \subseteq \mathbb{R}^{d_I}$ be an input space and \mathcal{Y} be a set of classes. The data points $x \in \mathcal{X}$ and corresponding classes $c \in \mathcal{Y}$ are sampled from the joint distribution \mathcal{D} . The feature mapping $f : \mathcal{X} \rightarrow \mathcal{Z}$ extracts feature vectors according to the inputs, where $\mathcal{Z} = \mathbb{R}^{d_F}$ is a raw feature space. In this work, we assume that this mapping is modeled by a neural network.

Softmax classification

The softmax classifier is commonly used in neural network-based classification tasks. The softmax classifier estimates the class probability $p(c|x)$, which is the probability that data point x belongs to class c , as follows:

$$p(c|x) = \frac{\exp(l_c(x))}{\sum_{y \in \mathcal{Y}} \exp(l_y(x))}, \tag{1}$$

where logit $l_y(x)$ is the neural network output according to input $x \in \mathcal{X}$ and class $y \in \mathcal{Y}$. Usually, logit $l_y(x)$ is calculated as:

$$l_y(x) = W_y^T f(x) + b_y, \tag{2}$$

where the feature vector $f(x)$ is an output of a penultimate layer, W_y is a weight vector, and b_y is a bias term for class y . The probability $p(c|x)$ estimated by the model is often called the confidence value (score). Based on the estimated class probabilities, we can use the cross-entropy loss to train the model. This loss measures the difference between the predicted and target probability distributions. The cross-entropy (CE) loss of a

mini-batch $B \subseteq \mathcal{D}$ is defined as:

$$L_{CE} = -\frac{1}{|B|} \sum_{(x_i, c_i) \in B} \log(p(c_i|x_i)). \quad (3)$$

Metric learning

While softmax classifiers are commonly used in deep learning classification, metric learning approaches can be beneficial, as they better control data points in embedding space. Hence, metric learning can provide information on the similarity between different data points. Metric learning approaches can be divided into two categories: (direct) embedding-based methods and classification-based methods. Embedding-based methods [19, 20] directly compare data points in embedding space to train an embedding function (feature map) $f(\cdot)$. Because embedding-based methods compare data points directly, they must be trained with pairs (using the contrastive loss) or triplets (using the triplet loss) of data points. Thus, embedding-based methods have high training complexity and require special mining algorithms [13] to prevent slow convergence speeds [14]. On the other hand, classification-based methods [13, 15, 16, 21, 22] use class representatives to represent classes. According to the classification loss (cross-entropy loss), class representatives guide data points to converge to class-specific positions. Classification-based methods converge faster than embedding-based methods due to their reduced sampling complexity (training with single data points). In this paper, we focus on classification-based metric learning methods.

NormFace

NormFace [13], which is also known as normalized softmax [23], modifies Eq. 2 in the softmax classifier. NormFace was motivated by the normalization of features during feature comparisons to improve face verification during the testing phase. To apply normalization during both the testing and training phases, NormFace normalizes the feature (embedding) vectors and weight vectors and uses a zero bias term. Previous experiments on metric learning models [8] have shown that NormFace and its variants [15, 16, 24] achieved competitive performance on metric learning tasks.

We denote $\tilde{v} = \frac{v}{\|v\|}$ for any nonzero vector v and the angle between vectors \tilde{W}_y and $\tilde{f}(x)$ as θ_y . Then, as $\|\tilde{W}_y\| = 1 = \|\tilde{f}(x)\|$, we obtain the following equation:

$$\tilde{W}_y^T \tilde{f}(x) = \|\tilde{W}_y\| \|\tilde{f}(x)\| \cos \theta_y = \cos \theta_y. \quad (4)$$

According to Eq. 4, the class probability $p(c|x)$ estimated by NormFace can be expressed as:

$$p(c|x) = \frac{\exp(s\tilde{W}_c^T \tilde{f}(x))}{\sum_{y \in \mathcal{Y}} \exp(s\tilde{W}_y^T \tilde{f}(x))} = \frac{\exp(s \cos \theta_c)}{\sum_{y \in \mathcal{Y}} \exp(s \cos \theta_y)}, \quad (5)$$

where $s > 0$ is a scaling factor. NormFace learns embeddings according to this estimation and the cross-entropy loss in Eq. 3.

We next investigate the geometrical meaning of the NormFace classification results. If a data point x is classified as belonging to class c by NormFace, according to Eq. 5, we obtain $\exp(s \cos \theta_c) \geq \exp(s \cos \theta_y)$, i.e., $\cos \theta_c \geq \cos \theta_y$. As the cosine function is a monotonically decreasing function in the interval $(0, \pi)$, we obtain $\theta_c \leq \theta_y$. In terms of angles, the normalized embedding vector $\tilde{f}(x)$ is closer (or equally close) to \tilde{W}_c than \tilde{W}_y . As we can classify data points using normalized weight vectors according to this

geometrical interpretation, we can consider \tilde{W}_y as the class representative for a class $y \in \mathcal{Y}$. Fig. 2 visualizes the above explanation.

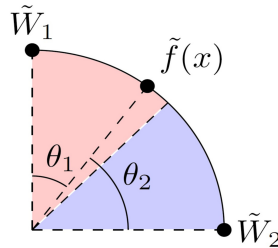


Fig 2. Visualization of NormFace classification results for two classes with $\tilde{W}_1=(\mathbf{0},1)$ and $\tilde{W}_2=(\mathbf{1},\mathbf{0})$. As $\tilde{f}(x)$ is closer to \tilde{W}_1 than \tilde{W}_2 , data point x is classified as belonging to class 1.

Proxies and prototypes

Although NormFace [13] uses a learnable weight vector as a class representative for each class, the average point for a class can also be used as a class representative. To prevent confusion, we define two kinds of class representatives for each class: a proxy representative and a prototype representative. We refer to the learnable weight vectors as proxy representatives. In NormFace, the weight vectors \tilde{W}_y are proxies. In this work, the proxy representatives are used to define the training loss and directly update the network. Note that we can predefine the proxy representatives, and the proxies can be fixed. On the other hand, we refer to the (normalized) average embedding for each class as a prototype representative. We denote the average embedding for class y as vector μ_y . In normalized space, this vector is defined as:

$$\mu_y = \frac{1}{|X_y|} \sum_{x \in X_y} \tilde{f}(x),$$

where $X_y \subseteq \mathcal{X}$ is a set of data points in class y . Then, the prototype representatives are defined as $\tilde{\mu}_y = \frac{\mu_y}{\|\mu_y\|}$. A metric learning method known as the prototypical network [9] was devised for few-shot learning tasks. During the training process, this network uses local prototypes based on special mini-batches known as episodes. In their work, the authors used unnormalized average embedding as prototypes because they considered Euclidean space. In this paper, we do not use prototypes for training, and (global) prototypes using training data are used only for evaluation.

Note that the proxy and prototype representatives are not necessarily the same. For instance, when we train the model with fixed proxies, the positions of the prototypes change during training, while the positions of the proxies remain fixed. Moreover, the confidence values are not necessarily maximized at the proxies [25]. In this case, the data points may not converge to their proxies. This concept is explained further in the next subsection.

SD softmax and DR formulation

In our previous work [25], we analyzed a softmax formulation for metric learning in which negative squared distances were used as logit values. We called this formulation the “softmax-based formulation” in our previous paper. In this work, we refer to this formulation as “squared distance (SD) softmax” to prevent confusion with the standard softmax formulation shown in Eq. 1.

We denote the class representative for class y as R_y and the distance to class y as $d_{x,y} := d(f(x), R_y)$ according to the distance function $d(\cdot, \cdot)$. For the normalized embeddings, we define $d_{x,y} := d(\tilde{f}(x), R_y)$ by assuming that point R_y is normalized. Then, the class probability $p(c|x)$ estimated using the SD softmax formulation is:

$$p(c|x) = \frac{\exp(-d_{x,c}^2)}{\sum_{y \in \mathcal{Y}} \exp(-d_{x,y}^2)}. \quad (6)$$

The SD softmax formulation uses the difference in the squared distance for training. Consider the following equation:

$$\|\tilde{W}_y - \tilde{f}(x)\|^2 = \|\tilde{W}_y\|^2 + \|\tilde{f}(x)\|^2 - 2\tilde{W}_y^T \tilde{f}(x) = 1 + 1 - 2 \cos \theta_y.$$

Then, we obtain:

$$s \cos \theta_y - s = -\frac{s}{2} \|\tilde{W}_y - \tilde{f}(x)\|^2.$$

Thus, we obtain the equation:

$$\frac{\exp(s \cos \theta_c)}{\sum_{y \in \mathcal{Y}} \exp(s \cos \theta_y)} = \frac{\exp(s \cos \theta_c - s)}{\sum_{y \in \mathcal{Y}} \exp(s \cos \theta_y - s)} = \frac{\exp(-\frac{s}{2} \|\tilde{W}_c - \tilde{f}(x)\|^2)}{\sum_{y \in \mathcal{Y}} \exp(-\frac{s}{2} \|\tilde{W}_y - \tilde{f}(x)\|^2)}, \quad (7)$$

(This equation is taken from [13]). The above equation shows that the NormFace formulation in Eq. 5 can be considered an SD softmax formulation 6 that uses the Euclidean distance on a hypersphere with radius $\sqrt{\frac{s}{2}}$.

In [25], we found that the SD softmax formulation had two main limitations. First, the estimated probability and corresponding loss may be affected by scaling changes. However, while this limitation must be considered when a Euclidean space is used, this limitation can be addressed by using normalized embeddings, as in the NormFace model [13]. The second limitation is that the estimated class probabilities are not optimized at the class representatives. For instance, the maximum estimated class probability $p(c|x)$ is not found at the class representative of class c . The NormFace model also encounters this issue. In the example shown in Fig. 2 with scaling factor $s = 2$, point $(-\frac{1}{\sqrt{2}}, \frac{1}{\sqrt{2}})$ is the point that maximizes the confidence value of class 1.

To address the above limitations, we proposed the distance ratio (DR)-based formulation [25] for metric learning models. Mathematically, the DR formulation estimates the class probability $p(c|x)$ as:

$$p(c|x) = \frac{\frac{1}{d_{x,c}^s}}{\sum_{y \in \mathcal{Y}} \frac{1}{d_{x,y}^s}} = \frac{d_{x,c}^{-s}}{\sum_{y \in \mathcal{Y}} d_{x,y}^{-s}}. \quad (8)$$

The DR formulation uses ratios of distances for training.

Moreover, the DR formulation [25] resolves the above two limitations of the SD softmax formulation. In the example shown in Fig. 2, for any scaling factor s , point $(0, 1) = \tilde{W}_1$ is the point that maximizes the confidence value of class 1. Thus, our experiments showed that the DR formulation has faster or comparable training speed in Euclidean (unnormalized) embedding spaces.

Exponential moving average (EMA) approach

Zhe et al. [21] theoretically showed that, while training NormFace [13], the commonly used gradient descent update method for the proxies based on the training loss cannot guarantee that the updated proxies approach the corresponding prototypes. To address this issue, they proposed using the normalized exponential moving average (EMA) to update the proxies. Mathematically, when updating a proxy for a data point x in class c , the proxy \tilde{W}_c is updated as:

$$\tilde{W}_c := \frac{\alpha \tilde{f}(x) + (1 - \alpha) \tilde{W}_c}{\left\| \alpha \tilde{f}(x) + (1 - \alpha) \tilde{W}_c \right\|}, \quad (9)$$

where $0 < \alpha < 1$ is a parameter that controls the speed and stability of the updates. Their experimental results showed that the EMA approach achieved better performance than the standard NormFace model on multiple datasets.

Adaptive scaling factor approach

Based on previous observations that the convergence and performance of NormFace models [13] depend on the scale parameter s , Zhang et al. [22] proposed AdaCos, which is a NormFace model trained by using the adaptive scale factor s in Eq. (5). Moreover, they suggested to use parameter s , which significantly changes the probability $p(c|x)$ estimated by Eq. (5), where c is the class of data point x . In other words, they attempted to find a parameter s that maximizes $\left\| \frac{\partial p(c|x)(\theta_c)}{\partial \theta_c} \right\|$ by approximating an s value that satisfies the equation:

$$\left\| \frac{\partial^2 p(c|x)(\theta'_c)}{\partial \theta_c'^2} \right\| = 0, \quad (10)$$

where $\theta'_c := \text{clip}(\theta_c, 0, \frac{\pi}{2})$ and $\text{clip}(\cdot, \cdot, \cdot)$ is a function that limits a value within a specified range. They proposed two AdaCos models: static (fixed) and dynamic versions. The static model determines a good scale parameter s before training the NormFace model based on observations of the angles between the data points and proxies. In the static model, the scale parameter s is not updated. The dynamic model updates the scale parameter s during each iteration based on the current angles between the data points and proxies.

CORR loss

In contrast to previous metric learning approaches that ignored hierarchical relationships among classes, Barz and Denzler [5] used normalized embeddings to achieve hierarchy-informed classification. First, they predefined the positions of the proxies using a given hierarchical structure. These proxies are fixed, i.e., they are not updated during training. Then, they used the predefined proxies to train the models according to the CORR loss. For a data point x in class c , the CORR loss ensures that the embedding vector $\tilde{f}(x)$ is close to the corresponding proxy \tilde{W}_c . The CORR loss of a mini-batch $B \subseteq \mathcal{D}$ is defined as:

$$L_{CORR} = \frac{1}{|B|} \sum_{(x_i, c_i) \in B} \left(1 - \tilde{W}_{c_i}^T \tilde{f}(x_i) \right) = \frac{1}{|B|} \sum_{(x_i, c_i) \in B} (1 - \cos \theta_{c_i}), \quad (11)$$

where θ_{c_i} is the angle between \tilde{W}_{c_i} and $\tilde{f}(x_i)$.

Methods

We investigated several methods and training options. The details of the settings are described in the following sections. The codes for our experiments will be available in https://github.com/hjk92g/Inspecting_Hierarchies_ML.

Dataset We conducted experiments using three plankton datasets (small microplankton, large microplankton, and mesozooplankton) and two benchmark datasets (CIFAR100 [26] and NABirds [27]). Table 1 summarizes the number of classes and images in each dataset. The three plankton datasets were obtained from the Institute of Marine Research (IMR), where flow imaging microscopy is used during routine monitoring. The plankton samples were imaged using three FlowCams, ©2022 Yokogawa Fluid Imaging Technologies, Inc., with different magnification settings. The three plankton datasets contain nonliving classes of artifacts and debris. Moreover, these datasets contain class names that are not in the WordNet database [11]. In addition, the three plankton datasets have severe class imbalances. For example, each class in the small microplankton (MicroS) dataset contains 1 to 456 images. Further details on the plankton datasets can be found in S2 Appendix. We randomly divided each plankton dataset into 70% training data, 10% validation data, and 20% test data. For the plankton datasets, we use images without any augmentation. As the input images have diverse image sizes, we resized the input images to 128×128 . The CIFAR100 dataset contains 100 classes and 600 images per class. The CIFAR100 contains 50000 training and 10000 test images, and we randomly divided the original training data into 45000 training and 5000 validation data. Furthermore, we applied random transformations (15 degree range rotations, 10% range translations, 10% range scaling, 10 degree range shearing, and horizontal flips) on the CIFAR100 training data. We did not resize images from their original size of 32×32 . The NABirds dataset contains 23929 training and 24633 test images. Similar to the plankton datasets, we randomly divided this dataset into 70% training data, 10% validation data, and 20% test data. We resized the images to 128×128 pixels. We also applied the same augmentations applied to the CIFAR100 dataset on the NABirds dataset. The predefined hierarchical structures are available in S1 Appendix.

Table 1. Summary of the studied datasets.

Dataset	Target particle (plankton datasets)	Images per class	Images	Classes
Small microplankton (MicroS)	5 to 50 μm	1 to 456	6738	109
Large microplankton (MicroL)	35 to 500 μm	2 to 613	8348	102
Mesozooplankton (MesoZ)	180 to 2000 μm	3 to 486	6738	52
CIFAR100 [26]	—	600	60000	100
NABirds [27]	—	13 to 120	48562	555

Models We consider four types of models: the softmax classifier, NormFace, ProxyDR (explained below), and a CORR loss-based model. We focus on metric learning models with normalized embeddings, as normalization is commonly used in metric learning models to improve performance [5, 13, 28]. ProxyDR is a model that uses

proxies for classification and DR formulations (8) to estimate class probabilities $p(c|x)$. Similar to the NormFace model, ProxyDR uses the Euclidean distance on a hypersphere. The difference between the two models is that ProxyDR uses DR formulations, while NormFace uses SD softmax formulations (as shown in Eq. 7). For the plankton datasets, we used a pretrained Inception version 3 architecture [29] as the backbone. For the CIFAR100 and NABirds datasets, we used a pretrained ResNet50 [30] as the backbone. In addition to the backbones, we applied a learnable linear transformation to obtain 128-dimensional embeddings $f(x)$. For the plankton datasets, we incorporate the size information. Specifically, when a data point x has size $v_{size} = [width, height]^T$, we take the elementwise logarithm $v'_{size} = [\log(width), \log(height)]^T$. By applying a linear transformation, we obtain an embedding vector $f_{size}(x)$ according to the size information, i.e., $f_{size}(x) = W_{size}^T v'_{size} + b_{size}$, where W_{size} is a learnable matrix with shape 2×128 and $b_{size} \in \mathbb{R}^2$ is a learnable vector. Then, we add this vector to the original embedding vector, namely, $f(x) := f(x) + f_{size}(x)$.

Training settings We trained the models according to the backbone weights and other weights (linear transformations, proxies). We used the Adam optimizer [31] with a learning rate of 10^{-4} . Except in the case of a dynamic approach (explained below), we use 10.0 as a scaling factor in both NormFace and ProxyDR. We set the training batch size in all experiments to 32. For the plankton datasets, we trained the models for 50 epochs. For the CIFAR100 and NABirds datasets, we trained the models for 100 epochs. During each epoch, we assessed the model accuracy. We chose the model with the highest validation accuracy for testing. For each setting, we trained the models five times with different seeds for the random split.

Training options The different training options are described as follows. The dynamic approach affects the scale factors in Eqs. 5 and 8. The EMA and MDS approaches both affect the proxy calculations.

- Standard: standard training with a fixed scale factor $s = 10$, with proxies updated using the cross-entropy loss (3).
- EMA (exponential moving average): training using the normalized exponential moving average [21], as shown in Eq. 9, to update the proxies. When multiple data points have the same class c in a mini-batch, we apply a modified expression. Specifically, instead of applying the EMA using a single data point, as in Eq. 9, we use the normalized average embedding (local prototype) of the mini-batch. Mathematically, when updating a proxy for m data points $x_{B;1}, \dots, x_{B;m}$ with class c in mini-batch B , the normalized average embedding is defined as:

$$\tilde{\mu}_{B;c} = \frac{\sum_{i=1}^m \tilde{f}(x_{B;i})}{\left\| \sum_{i=1}^m \tilde{f}(x_{B;i}) \right\|}.$$

Then, proxy \tilde{W}_c is updated as:

$$\tilde{W}_c := \frac{\alpha \tilde{\mu}_{B;c} + (1 - \alpha) \tilde{W}_c}{\left\| \alpha \tilde{\mu}_{B;c} + (1 - \alpha) \tilde{W}_c \right\|}, \quad (12)$$

where α is the same parameter as in Eq. 9. We set the parameter α to 0.001.

- **Dynamic:** training with a dynamic scale factor, similar to AdaCos [22]. In contrast to the original paper, which chooses a scale factor using an approximate expression, we use the Adam [31] optimizer to determine a scale factor that satisfies Eq. 10. More details are included in S1 Appendix.
- **MDS (multidimensional scaling):** training according to predefined hierarchical information. We use the hierarchical information to set (fixed) proxies. First, as in the distance calculation method in the problem setting subsection, we use a predefined hierarchy to generate a distance matrix. We denote the (hierarchical) distance between the i th and j th classes as $d_H(i, j)$. For each hierarchical distance d_H , we apply a transformation $d_T = \frac{\sqrt{2}d_H}{\beta+d_H}$ for a scalar $\beta > 0$ to address the limited Euclidean distance ($\leq \sqrt{2}$) on unit spherical spaces. We set $\beta = 1.0$ in all of our experiments. (Note that if d is a metric, the transformed distance $\frac{\sqrt{2}d}{\beta+d}$ is also a metric.) Then, according to the transformed distance matrix D_T , we use multidimensional scaling (MDS) to set the proxies. Mathematically, we minimize a value known as the normalized stress, which can be expressed as:

$$\text{Stress}(D_{\tilde{W}}) := \frac{\|D_{\tilde{W}} - D_T\|_F}{\|D_T\|_F}, \quad (13)$$

where $D_{\tilde{W}}$ is a pairwise Euclidean distance matrix according to proxies \tilde{W}_y and $\|\cdot\|_F$ is the Frobenius norm. We use the Adam optimizer with a learning rate of 10^{-3} for 1000 iterations to obtain the proxies. While we used stochastic gradient descent for the MDS option, different methods, such as those applied by Barz and Denzler [5], can also be used for MDS. During training, we fix the obtained proxies and update only the embedding function $f(\cdot)$.

Performance measures In our experiments, we consider three types of performance measures: standard classification measures, hierarchical inference performance measures, and hierarchy-informed performance measures. The hierarchical inference performance measures are used to estimate how well the learned class representatives match the predefined hierarchies. The hierarchy-informed performance measures are used to estimate how well a model performs on classification or similarity measures according to the predefined hierarchies.

We used the top- k accuracy as a standard classification measure, the mean correlation as the hierarchical inference performance measure, and the average hierarchical distance (AHD), hierarchical precision at k (HP@ k), hierarchical similarity at k (HS@ k), and average hierarchical similarity at k (AHS@ k) as hierarchy-informed performance measures. The utilized measures are defined as follows.

- **Top- k accuracy:** The classification accuracy was calculated, with correct classification defined as whether the labeled class is in the top- k predictions (most likely classes), i. e., the k classes with the highest confidence values. We report results for $k = 1, 5$.
- **Mean correlations:** We introduce this measure to evaluate how well the learned class representatives match the predefined hierarchical structure. We obtain the class representatives (either proxies or prototypes) from the learned model using training data points. Then, we obtain the pairwise distance matrix D_L based on the class representatives. We compare matrix D_L with the distance matrix D_H based on the predefined hierarchical structure. Specifically, for each class (row), we calculate Spearman’s rank correlation coefficient according to the two matrices.

Then, we determine the mean correlation using Fisher transformations. More precisely, we apply a Fisher transformation $\operatorname{arctanh}(\cdot)$ on each correlation coefficient, take the average of the transformed values, and apply $\operatorname{tanh}(\cdot)$ on the average value.

For the plankton datasets, the predefined hierarchical structures of the living classes are based on biological taxonomies. However, these datasets also contain some nonliving classes, such as “large bubbles” and “dark debris”. Considering that the predefined hierarchical structures of the living classes are scientifically defined, for the plankton datasets, we report mean correlations among whole classes or only among living classes.

- **AHD**: The average hierarchical distance of the top- k predictions [4] was calculated as the average hierarchical distance d_H between the labeled classes and each of the top- k most likely classes. In contrast to Bertinetto et al. [4], who considered only misclassified cases, we consider all cases. Hence, in our calculations, the final denominators differ. When $k = 1$, the AHD measure is the same as the average hierarchical cost (AHC) measure defined by Garnot and Landrieu [6]. We report results for $k = 1, 5$.
- **HP@ k** : The hierarchical precision at k [32] was taken as a performance measure. Specifically, let us denote a (hierarchical) neighborhood set of a class c with the distance threshold ϵ as $N(c, \epsilon)$, i.e., $n \in N(c, \epsilon) \iff d_H(c, n) \leq \epsilon$. We define $\text{hCorrectSet}(c, k)$ as the neighborhood set $N(c, \epsilon)$ with the smallest ϵ such that $|\text{hCorrectSet}(c, k)| \geq k$. Then, the hierarchical precision at k is calculated as the fraction of the top- k predictions in $\text{hCorrectSet}(c, k)$. We report the results for $k = 5$.
- **HS@ k** : The hierarchical similarity at k is a measure that was introduced by Barz and Denzler [5] with the name “hierarchical precision at k ”, although this metric does not evaluate precision and instead assesses similarity. Here, we use a different measure with the same name that was defined by Frome et al. [32]. Hence, we renamed the measure “hierarchical similarity at k ”. When c is a label of a query data point x , let $R = ((x_1, c_1), \dots, (x_m, c_m))$ be the ordered list of image-label pairs based on the distance (sorted by ascending distance) to point x in the normalized embedding space. Considering $\cos(\theta) = 1 - \frac{\|u_1 - u_2\|_2^2}{2}$, where u_1 and u_2 are unit vectors and θ is the angle between u_1 and u_2 , we defined the similarity between the i th and j th classes $s_H(i, j)$ as:

$$s_H(i, j) = 1 - \frac{d_T(i, j)^2}{2}, \quad (14)$$

where i and j are the indices for classes ($1 \leq i, j \leq |\mathcal{Y}|$).

The hierarchical similarity at k is then defined as:

$$HS@k := \frac{\sum_{i=1}^k s_H(I(c), I(c_i))}{\max_{\pi} \sum_{i=1}^k s_H(I(c), I(c_{\pi_i}))}, \quad (15)$$

where $I(\cdot)$ is an index function that outputs the corresponding index (between 1 and $|\mathcal{Y}|$) for a class and π is an index permutation that ranges from 1 to m . We report results for $k = 50, 250$.

- **AHS@ K** : The average hierarchical similarity at K was introduced by Barz and Denzler [5] as the “average hierarchical precision at K ”. Due to similar reasons as

for $HS@k$, we renamed the measure. The average hierarchical similarity at K is defined as the area under the curve of $HS@k$ from $k = 1$ to $k = K$. We report results for $K = 250$.

Results

Main results

The performance measure evaluation results are shown in bar plots with 95% confidence intervals. Dashed lines separate models trained with or without predefined hierarchical knowledge. We show only the results on the CIFAR100 and NABirds datasets in the main text. All results are included in S3 Appendix. To reduce spurious findings, we focus on consistent trends across the five datasets.

Figs. 3 and 4 and the figures in S3 Appendix show the top- k accuracy for various training settings. The NormFace and ProxyDR models achieved comparable top- k accuracy for both k values on most datasets. The softmax loss model obtained low top- k accuracy. While the result was not significant, using the dynamic option achieved higher top-1 accuracy than standard training. When the EMA option was added to the standard and dynamic options, the top-5 accuracy decreased, except for standard NormFace on the NABirds dataset. While the CORR loss achieved top-1 accuracy that was comparable to that achieved by other training options with predefined hierarchical information, this model obtained low top-5 accuracy on all datasets. The top-5 accuracy with the CORR loss was even lower than that with the softmax loss, except on the NABirds dataset. Although the results were better than those of the CORR loss model, the use of predefined hierarchical information during training for NormFace and ProxyDR also reduced the top-5 accuracy. These results show the opposite trend to the changes in the top-1 accuracy, which showed comparable or enhanced performance. Moreover, the dynamic MDS approach obtained lower top-5 accuracy than the MDS approach without the dynamic option.

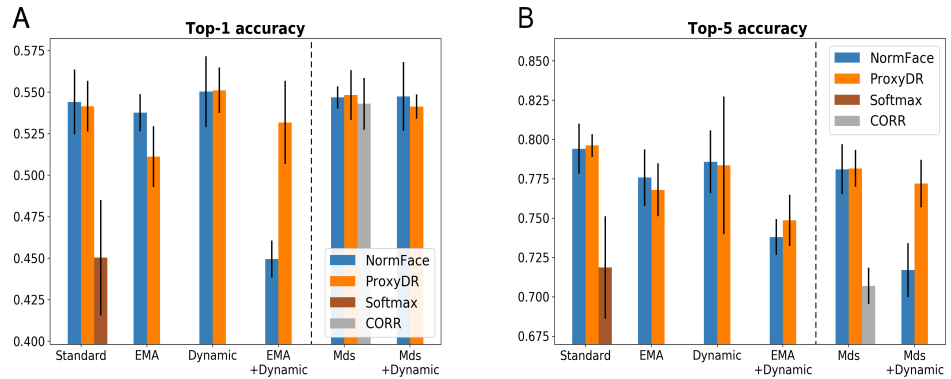


Fig 3. Top- k accuracy results (A: $k = 1$, B: $k = 5$) on the CIFAR100 dataset.

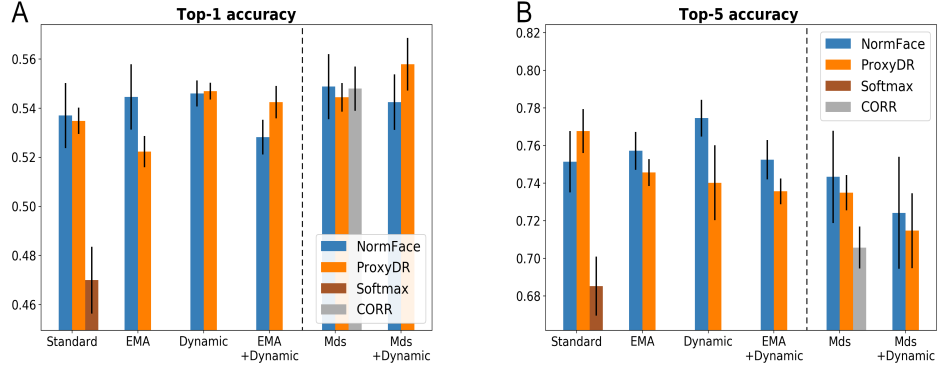


Fig 4. Top- k accuracy results (A: $k = 1$, B: $k = 5$) on the NABirds dataset.

Figs. 5 and 6 and the figures in S3 Appendix show the mean correlation values for various training options. When we consider training options that do not use predefined hierarchical information, ProxyDR obtains higher mean correlations than NormFace, except for the EMA approaches. The ProxyDR model with the dynamic option obtained higher mean correlations than the standard ProxyDR model. As expected, the use of predefined hierarchical information greatly increased the mean correlations based on prototypes in both the NormFace and ProxyDR models, except the ProxyDR model on the NABirds dataset. When we consider training options that utilize predefined hierarchical information, the CORR loss model achieved the highest mean correlations based on prototypes in most cases. The ProxyDR model typically achieved the second-best mean correlations.

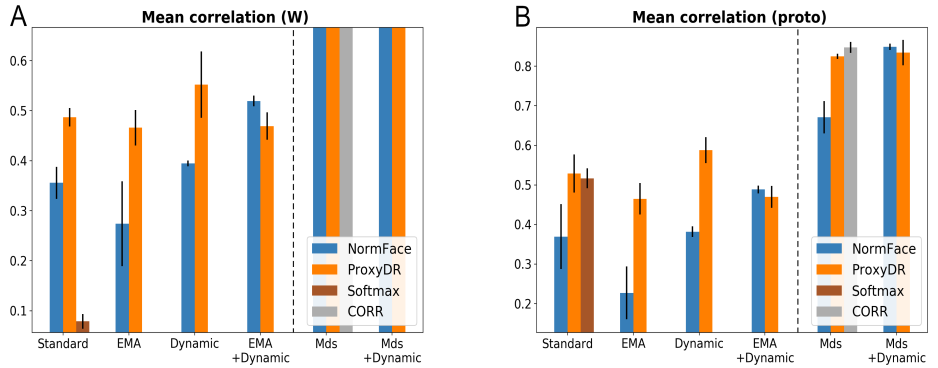


Fig 5. Correlation measures on the CIFAR100 dataset. (A) Values using proxies. (B) Values using prototypes. The mean correlation value based on proxies with the MDS option was 0.8580.

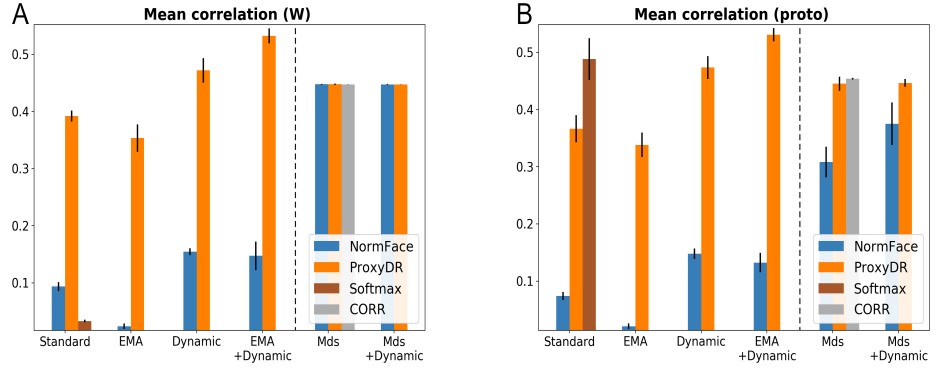


Fig 6. Correlation measures on the NABirds dataset. (A) Values using proxies. (B) Values using prototypes. The mean correlation value based on proxies with the MDS option was 0.4476 (this value is small because the dataset contains 555 classes and the embedding dimension is 128.).

Figs. 7 and 8 and the figures in S3 Appendix show the hierarchical performance measures obtained with various training options. The softmax loss option achieved the worst hierarchical performance, except for AHS@50 on the NABirds dataset. Although these measures are used to assess the hierarchy-informed performance, some of the measures are not substantially affected by the use of predefined hierarchical information during training. For instance, the use of predefined hierarchical information in the CIFAR100 dataset (Fig. 7) did not show noticeable improvements in terms of the AHD ($k=1$), HS@50, and AHS@250 measures. Moreover, while the use of predefined hierarchical information significantly improved the HS@250 results on most datasets, only marginal improvements were observed for the CIFAR100 dataset. On the other hand, the use of predefined hierarchical information significantly improved the AHD ($k=5$) and HP@5 results on all datasets. The CORR loss achieved the best results on these two measures, except on the NABirds dataset. Adding the dynamic option to the standard and MDS options improved performance on these two measures, except for the ProxyDR model on the CIFAR100 dataset. When we consider training options that do not use predefined hierarchical information, the ProxyDR model shows better performance than NormFace in terms of these two measures, except for the EMA and dynamic options on the CIFAR100 dataset. Under the same settings, ProxyDR performed better than NormFace in terms of the HS@250 measure, except for the EMA option on the CIFAR100 dataset. Moreover, under the same settings, the ProxyDR model with the dynamic option achieved the highest HS@250 and AHS@250 values among the compared models.

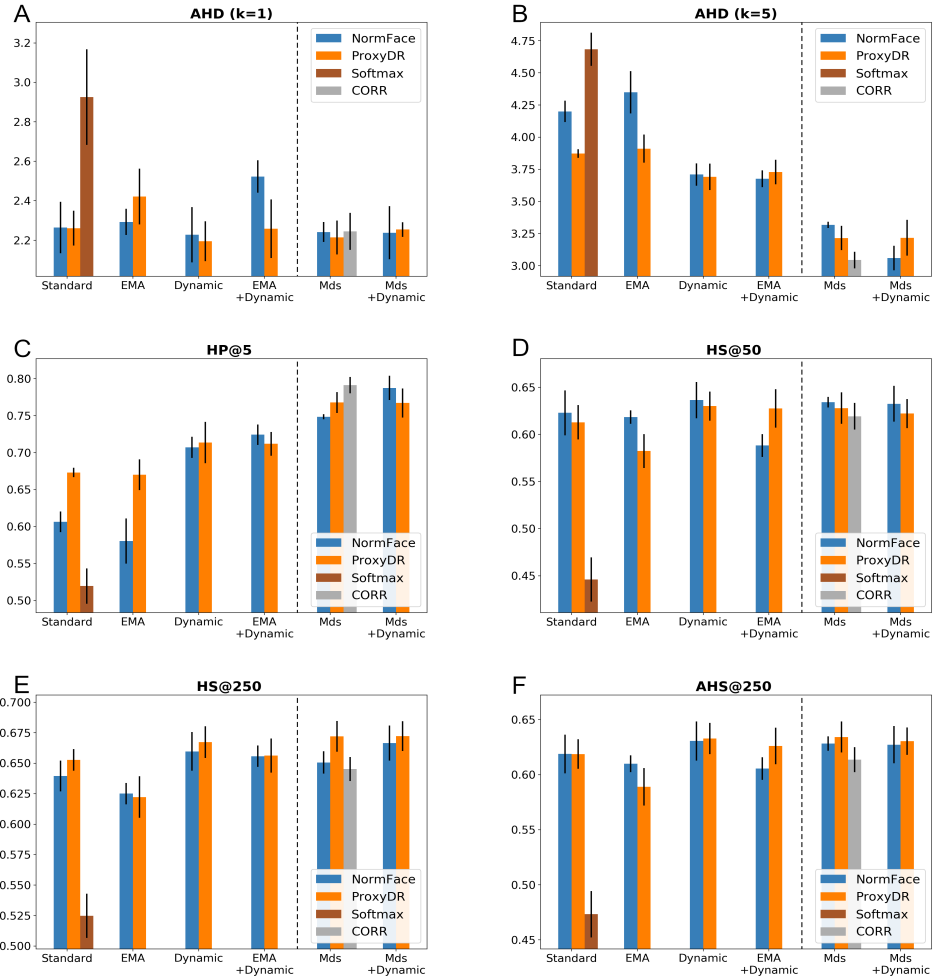


Fig 7. Hierarchical performance measures on the CIFAR100 dataset. The symbol \downarrow denotes that lower values indicate better performance. The symbol \uparrow denotes that higher values indicate better performance. (A) AHD (k=1): \downarrow . (B) AHD (k=5): \downarrow . (C) HP@5: \uparrow . (D) HS@50: \uparrow . (E) HS@250: \uparrow . (F) AHS@250: \uparrow .

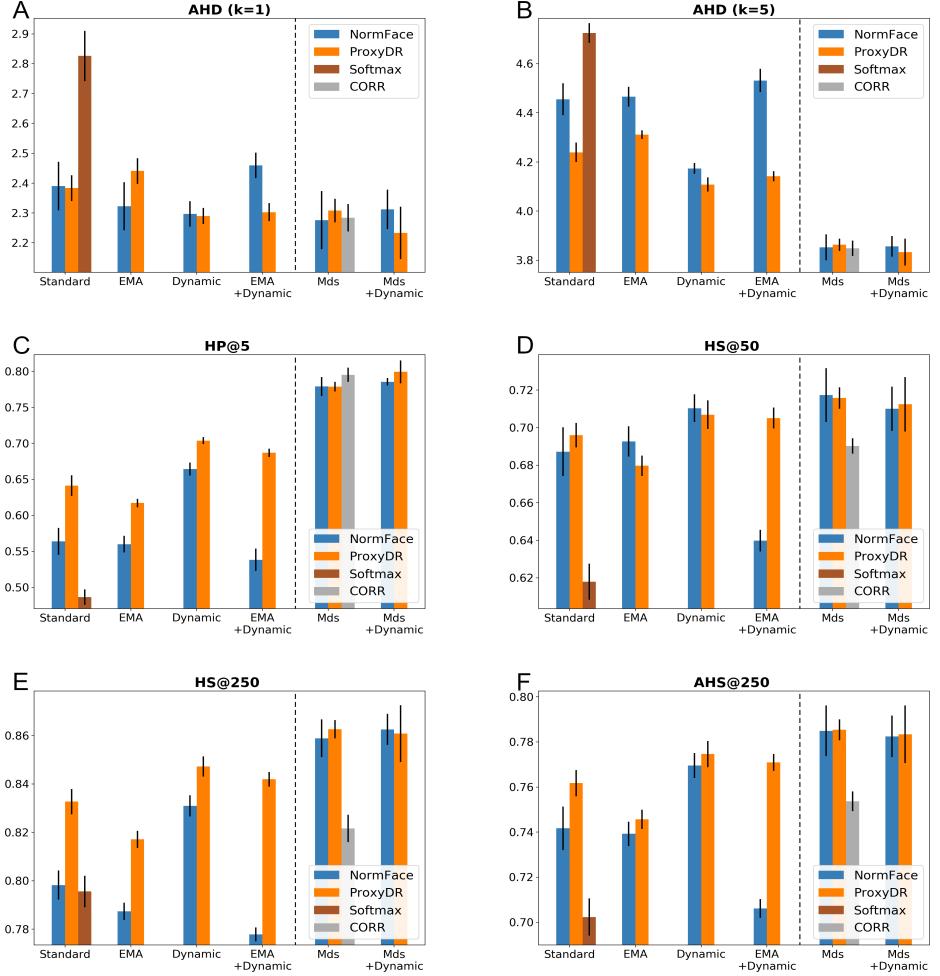


Fig 8. Hierarchical performance measures on the NABirds dataset. The symbol \downarrow denotes that lower values indicate better performance. The symbol \uparrow denotes that higher values indicate better performance. (A) AHD ($k=1$): \downarrow . (B) AHD ($k=5$): \downarrow . (C) HP@5: \uparrow . (D) HS@50: \uparrow . (E) HS@250: \uparrow . (F) AHS@250: \uparrow .

Additional mean correlation results

To investigate the changes in the class representatives, we evaluated the mean correlations at the end of each training epoch. We report only the results on the CIFAR100 and NABirds datasets. Moreover, we report results for ProxyDR models with the standard and dynamic options. More results are included in S3 Appendix. Furthermore, we report mean correlations based on random networks, i.e., networks with random weights, pretrained networks, and unnormalized and normalized input spaces.

Figs. 9 and 10 visualize the changes in the mean correlation values during ProxyDR model training (averaged values from five different seeds). Surprisingly, we found that the prototypes of the approximately untrained networks (pretrained on ImageNet [3] and trained on the target dataset, e.g., CIFAR100 or NABirds, for only one epoch) already have relatively high correlations (approximately 0.4), with predefined hierarchical structures. While the accuracy curves show no noticeable differences, using the dynamic option modified the transition in the mean correlations. In particular,

prototype-based mean correlations increased after 20 to 40 training epochs, and the maximum values were obtained near the end of training (approximately 100 epochs). The proxy-based mean correlations started at low values, and the difference with the prototype-based mean correlations was reduced. Moreover, the training epoch during which the validation accuracy is maximized often differs from the training epoch during which the correlation measures are maximized.

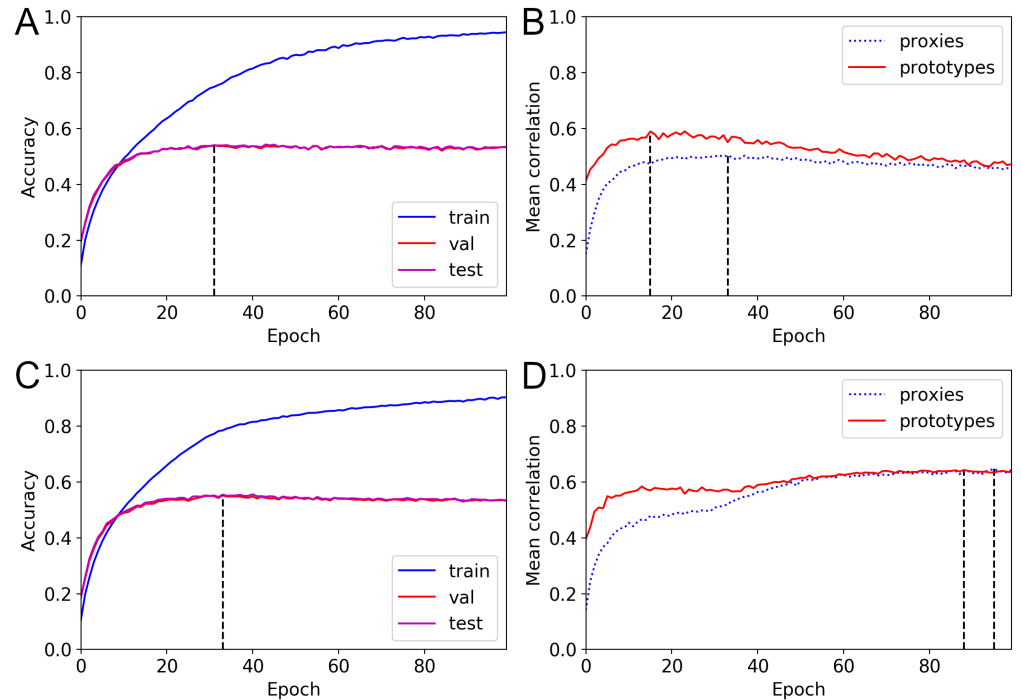


Fig 9. Changes in accuracy and mean correlations for the CIFAR100 dataset (ProxyDR). (A) Accuracy curve with standard training. (B) Mean correlation curve with standard training. (C) Accuracy curve with the dynamic option. (D) Mean correlation curve with the dynamic option.

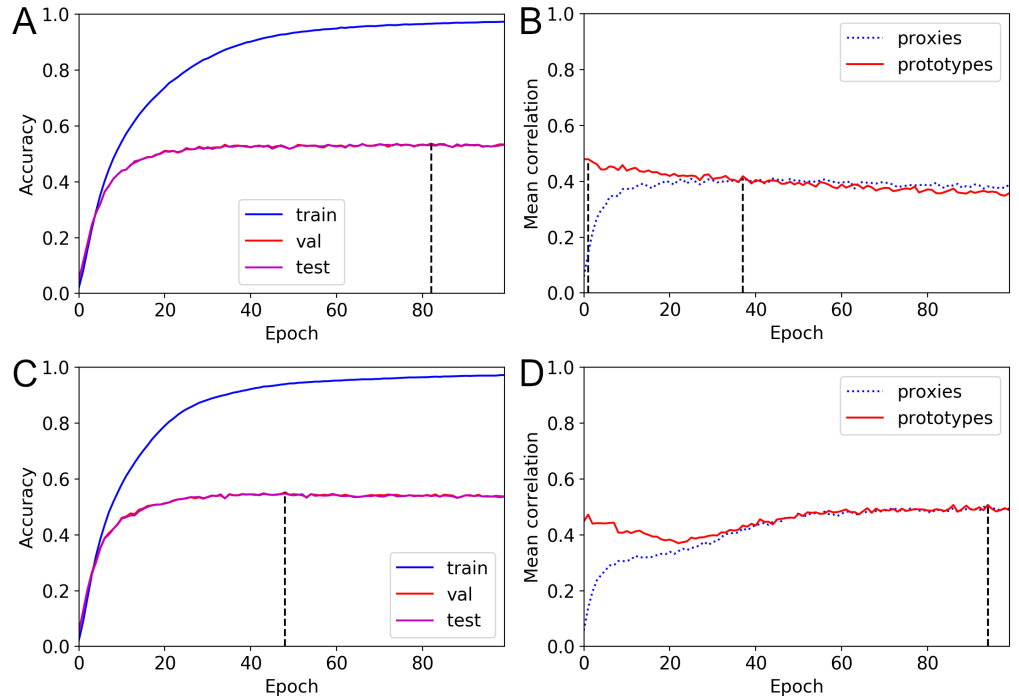


Fig 10. Changes in accuracy and mean correlations for the NABirds dataset (ProxyDR). (A) Accuracy curve with standard training. (B) Mean correlation curve with standard training. (C) Accuracy curve with the dynamic option. (D) Mean correlation curve with the dynamic option.

Table 2 shows prototype-based mean correlation values and their 95 percent confidence intervals based on five different seeds. The mean correlations with the random networks show that the prototypes and ground-truth hierarchy are correlated. While these values are smaller than the other cases shown in the table, the results show that random networks have some degree of semantic understanding.

Table 2. Mean correlations based on prototypes.

Space	Random weights	Pretrained	Input space	Normalized input space
CIFAR100	0.2841 ± 0.0303	0.3816 ± 0.0116	0.3414 ± 0.0353	0.2609 ± 0.0416
NABirds	0.1088 ± 0.0839	0.2648 ± 0.0349	0.1740 ± 0.0056	0.2369 ± 0.0039

“Random weights” and “pretrained” mean embedding space based on the ResNet50 [30] backbone.

Discussion

In this work, we investigate classification and hierarchical performance under different models and training options. Our experiments reveal several important findings. Under the training options that do not consider predefined hierarchical information, the ProxyDR model achieved better hierarchical inference performance than NormFace in most cases. Furthermore, under the same training options, ProxyDR achieved better hierarchy-informed performance in terms of the AHD ($k=5$) and HP@5 measures. Moreover, we observed that the use of a dynamic scaling factor improved the hierarchical inference performance. The changes in the mean correlation values (Figs. 9

and 10) verified the effect of the dynamic training option. These results reveal the importance of dynamic training approach. We also found that some hierarchy-informed performance measures are not significantly improved by the use of known hierarchical structures. This finding indicates that multiple hierarchy-informed performance measures should be considered to compare the hierarchy-informed performance of different models. We also observed a trade-off between the hierarchy-informed performance and top-5 accuracy. While the CORR loss model typically achieved the best hierarchical performance, this model obtained the lowest top-5 accuracy among the experimental models. Similarly, the use of predefined hierarchical information in NormFace and ProxyDR significantly improved the AHD (k=5) and HP@5 performance but reduced the top-5 accuracy. In contrast to previous works that observed a trade-off between hierarchy-informed performance and top-1 accuracy [4], we did not observe this trade-off with top-1 accuracy.

Surprisingly, we found that prototypes based on CNNs with random weights showed correspondence with predefined hierarchies that was higher than random chance. Because CNNs combine convolutional and pooling layers, most CNN architectures have translation invariance properties. Because of such priors, random networks may know weak perceptual similarity [33]. Another possible reason for this result is that prototypes of input spaces show higher correspondence with predefined hierarchies than random chance. The Johnson-Lindenstrauss lemma [34] shows that linear projections using random matrices approximately preserve distances. If this property holds for nonlinear projections based on random neural networks, network-based prototypes may also correspond to predefined hierarchies. This phenomenon suggests that when we use metric learning models with proxies, the proxies can be assigned based on prototypes instead of starting at random positions. This may improve training during the initial epochs, as we start from proxies that are more semantically reasonable than random positions.

Although we observed that the DR formulation improves the hierarchical inference performance and hierarchy-informed performance when training models without predefined hierarchies, we did not study the reasons underlying these phenomena. We suggest one possible hypothesis. While NormFace prevents sudden changes in the scaling factor by using normalized embeddings, its loss function is based on the squared difference of the distance (as it uses the SD softmax formulation). As this loss can increase the squared difference of the distance among different proxies, the absolute distance between any pairs of proxies may be increased. This tendency can result in larger distances, even among semantically similar classes, and proxy positions that are less organized in terms of visual similarity. On the other hand, the DR formulation-based loss is based on distance ratios. Thus, there is no tendency to increase absolute distances among proxies, and proxies can be structured according to visual similarity. However, further investigations are needed to verify this hypothesis and reveal the underlying cause.

Conclusion

The hierarchy-informed performance must be improved to more broadly adopt classification models. We explored this concept with classification-based metric learning models in situations in which hierarchical information is and is not available during training. Our results show that when the class hierarchical relations are unknown, the ProxyDR model achieves the best hierarchical inference and hierarchy-informed performance. In contrast, with hierarchy-informed training, the CORR loss model achieves the best hierarchy-informed performance but the lowest top-5 accuracy on most datasets. Since some hierarchy-informed measures may not be improved by the use of

hierarchical information during training, multiple hierarchy-informed performance measures should be used to obtain appropriate comparisons. Additionally, our experiments reveal that during classification-based metric learning, initializing proxies based on prototypes may be beneficial.

Acknowledgments

Hyeongji Kim, Terje Berge, and Ketil Malde acknowledge the Ministry of Trade, Industry and Fisheries for financial support. The authors thank Gayantonia Franze, Hege Lyngv er Mathisen, Magnus Reeve, and Mona Ring Kleiven, from the Plankton Research Group at Institute of Marine Research (IMR), for their contributions to the plankton datasets.

References

1. He K, Zhang X, Ren S, Sun J. Delving deep into rectifiers: Surpassing human-level performance on imagenet classification. In: Proceedings of the IEEE international conference on computer vision; 2015. p. 1026–1034.
2. Russakovsky O, Deng J, Su H, Krause J, Satheesh S, Ma S, et al. Imagenet large scale visual recognition challenge. *International journal of computer vision*. 2015;115(3):211–252.
3. Deng J, Dong W, Socher R, Li LJ, Li K, Fei-Fei L. Imagenet: A large-scale hierarchical image database. In: 2009 IEEE conference on computer vision and pattern recognition. Ieee; 2009. p. 248–255.
4. Bertinetto L, Mueller R, Tertikas K, Samangooei S, Lord NA. Making better mistakes: Leveraging class hierarchies with deep networks. In: Proceedings of the IEEE/CVF Conference on Computer Vision and Pattern Recognition; 2020. p. 12506–12515.
5. Barz B, Denzler J. Hierarchy-based image embeddings for semantic image retrieval. In: 2019 IEEE Winter Conference on Applications of Computer Vision (WACV). IEEE; 2019. p. 638–647.
6. Garnot VSF, Landrieu L. Leveraging Class Hierarchies with Metric-Guided Prototype Learning. In: British Machine Vision Conference (BMVC); 2021.
7. Jayathilaka M, Mu T, Sattler U. Ontology-based n-ball concept embeddings informing few-shot image classification. *arXiv preprint arXiv:210909063*. 2021;.
8. Musgrave K, Belongie S, Lim SN. A metric learning reality check. In: European Conference on Computer Vision. Springer; 2020. p. 681–699.
9. Snell J, Swersky K, Zemel R. Prototypical Networks for Few-shot Learning. *Advances in Neural Information Processing Systems*. 2017;30:4077–4087.
10. Chen WY, Liu YC, Kira Z, Wang YCF, Huang JB. A closer look at few-shot classification. *arXiv preprint arXiv:190404232*. 2019;.
11. Miller GA. *WordNet: An electronic lexical database*. MIT press; 1998.
12. Godbole S. Exploiting confusion matrices for automatic generation of topic hierarchies and scaling up multi-way classifiers. *Annual Progress Report, Indian Institute of Technology–Bombay, India*. 2002;.

13. Wang F, Xiang X, Cheng J, Yuille AL. Normface: L2 hypersphere embedding for face verification. In: Proceedings of the 25th ACM international conference on Multimedia; 2017. p. 1041–1049.
14. Kim S, Kim D, Cho M, Kwak S. Proxy anchor loss for deep metric learning. In: Proceedings of the IEEE/CVF Conference on Computer Vision and Pattern Recognition; 2020. p. 3238–3247.
15. Wang H, Wang Y, Zhou Z, Ji X, Gong D, Zhou J, et al. Cosface: Large margin cosine loss for deep face recognition. In: Proceedings of the IEEE conference on computer vision and pattern recognition; 2018. p. 5265–5274.
16. Deng J, Guo J, Xue N, Zafeiriou S. Arcface: Additive angular margin loss for deep face recognition. In: Proceedings of the IEEE/CVF Conference on Computer Vision and Pattern Recognition; 2019. p. 4690–4699.
17. Wan A, Dunlap L, Ho D, Yin J, Lee S, Petryk S, et al. {NBDT}: Neural-Backed Decision Tree. In: International Conference on Learning Representations; 2021. Available from: <https://openreview.net/forum?id=mCLVvEpp1NE>.
18. Silla CN, Freitas AA. A survey of hierarchical classification across different application domains. *Data Mining and Knowledge Discovery*. 2011;22(1):31–72.
19. Weinberger KQ, Blitzer J, Saul L. Distance metric learning for large margin nearest neighbor classification. *Advances in neural information processing systems*. 2005;18.
20. Hadsell R, Chopra S, LeCun Y. Dimensionality reduction by learning an invariant mapping. In: 2006 IEEE Computer Society Conference on Computer Vision and Pattern Recognition (CVPR'06). vol. 2. IEEE; 2006. p. 1735–1742.
21. Zhe X, Ou-Yang L, Yan H. Improve L2-normalized Softmax with Exponential Moving Average. In: 2019 International Joint Conference on Neural Networks (IJCNN). IEEE; 2019. p. 1–7.
22. Zhang X, Zhao R, Qiao Y, Wang X, Li H. Adacos: Adaptively scaling cosine logits for effectively learning deep face representations. In: Proceedings of the IEEE/CVF Conference on Computer Vision and Pattern Recognition; 2019. p. 10823–10832.
23. Zhai A, Wu HY. Classification is a strong baseline for deep metric learning. *British Machine Vision Conference (BMVC)*. 2019;.
24. Liu W, Wen Y, Yu Z, Li M, Raj B, Song L. Sphereface: Deep hypersphere embedding for face recognition. In: Proceedings of the IEEE conference on computer vision and pattern recognition; 2017. p. 212–220.
25. Kim H, Parviainen P, Malde K. Distance-Ratio-Based Formulation for Metric Learning. *arXiv preprint arXiv:220108676*. 2022;.
26. Krizhevsky A. Learning multiple layers of features from tiny images; 2009.
27. Van Horn G, Branson S, Farrell R, Haber S, Barry J, Ipeirotis P, et al. Building a bird recognition app and large scale dataset with citizen scientists: The fine print in fine-grained dataset collection. In: Proceedings of the IEEE Conference on Computer Vision and Pattern Recognition; 2015. p. 595–604.

28. Movshovitz-Attias Y, Toshev A, Leung TK, Ioffe S, Singh S. No fuss distance metric learning using proxies. In: Proceedings of the IEEE International Conference on Computer Vision; 2017. p. 360–368.
29. Szegedy C, Vanhoucke V, Ioffe S, Shlens J, Wojna Z. Rethinking the inception architecture for computer vision. In: Proceedings of the IEEE conference on computer vision and pattern recognition; 2016. p. 2818–2826.
30. He K, Zhang X, Ren S, Sun J. Deep residual learning for image recognition. In: Proceedings of the IEEE conference on computer vision and pattern recognition; 2016. p. 770–778.
31. Kingma DP, Ba J. Adam: A method for stochastic optimization. arXiv preprint arXiv:1412.6980. 2014;.
32. Frome A, Corrado GS, Shlens J, Bengio S, Dean J, Ranzato M, et al. Devise: A deep visual-semantic embedding model. Advances in neural information processing systems. 2013;26.
33. Zhang R, Isola P, Efros AA, Shechtman E, Wang O. The unreasonable effectiveness of deep features as a perceptual metric. In: Proceedings of the IEEE conference on computer vision and pattern recognition; 2018. p. 586–595.
34. Johnson W, Lindenstrauss J. Extensions of Lipschitz mappings into a Hilbert space. Contemporary Mathematics. 1984;26:189–206.

Supporting information

S1 Appendix

Detailed explanation of the dynamic (adaptive) scaling factors in the NormFace and ProxyDR models.

Zhang et al. [22] rewrote Eq. 5 as follows:

$$p(c|x) = \frac{\exp(s \cos \theta_c)}{\exp(s \cos \theta_c) + B_x},$$

where c is the corresponding class of point x and $B_x = \sum_{y \neq c, y \in \mathcal{Y}} \exp(s \cos \theta_y)$. They found that θ_y was close to $\frac{\pi}{2}$ during the training process for $y \neq c$, i.e., for different classes. Thus, $B_x \approx \sum_{y \neq c, y \in \mathcal{Y}} \exp(s \cos \frac{\pi}{2}) = \sum_{y \neq c, y \in \mathcal{Y}} \exp(0) = |\mathcal{Y}| - 1$.

In Eq. 10, $\frac{\partial^2 p(c|x)(\theta_c)}{\partial \theta_c^2}$ can be written as:

$$\frac{\partial^2 p(c|x)(\theta_c)}{\partial \theta_c^2} = \frac{-s B_x \exp(s \cos \theta_c) \psi_{NormFace}(s, \theta_c)}{(\exp(s \cos \theta_c) + B_x)^3},$$

where $\psi_{NormFace}(s, \theta_c) = \cos \theta_c (\exp(s \cos \theta_c) + B_x) + s \sin^2 \theta_c (\exp(s \cos \theta_c) - B_x)$. Moreover, they used $s = \frac{\log B_x}{\cos \theta_c}$ to approximate the solution for Eq. 10. For the static version, they used $|\mathcal{Y}| - 1$ to estimate B_x and $\frac{\pi}{4}$ to estimate θ_c . For the dynamic version, they used $B_{x;avg}$ to estimate B_x and $\theta_{c;med}$ to estimate θ_c , where $B_{x;avg}$ is the average of B_x in a mini-batch and $\theta_{c;med}$ is the median of the θ_c values in a mini-batch. They clipped the $\theta_{c;med}$ value to be in the range $[0, \frac{\pi}{4}]$.

Instead of using $s = \frac{\log B_x}{\cos \theta_c}$, in our implementation, we use the Adam optimizer [31] to update a scale factor s that minimizes $\psi_{NormFace}^2(s, \theta_c)$, i.e., $\psi_{NormFace}(s, \theta_c) \approx 0$. For $\psi_{NormFace}(s, \theta_c)$, we use $|\mathcal{Y}| - 1$ to estimate B_x and $\frac{\pi}{4}$ to estimate θ_c to initialize the value of s . During model training, we use $B_{x;avg}$ to estimate B_x and $\theta_{c;med}$ to estimate θ_c .

We can also apply the dynamic scaling factor to the ProxyDR model. First, we define $d_{x,y} := \|\tilde{f}(x) - \tilde{W}_y\|$. We rewrite Eq. 8 as:

$$p(c|x) = \frac{d_{x,c}^{-s}}{d_{x,c}^{-s} + B_x},$$

where $B_x = \sum_{y \neq c, y \in \mathcal{Y}} d_{x,y}^{-s}$. Assuming $\theta_y \approx \frac{\pi}{2}$ for $y \neq c$, we obtain

$$B_x \approx \sum_{y \neq c, y \in \mathcal{Y}} \left(\frac{\pi}{2}\right)^{-s} = (|\mathcal{Y}| - 1) \left(\frac{\pi}{2}\right)^{-s}.$$

The expression $\frac{\partial^2 p(c|x)(\theta_c)}{\partial \theta_c^2}$ can be written as:

$$\frac{\partial^2 p(c|x)(\theta_c)}{\partial \theta_c^2} = \frac{B_x s \theta_c^{(s-2)} \psi_{ProxyDR}(s, \theta_c)}{(B_x \theta_c^s + 1)^3}$$

where $\psi_{ProxyDR}(s, \theta_c) = B_x (s + 1) \theta_c^s - s + 1$. We then use the Adam optimizer to update a scale factor s that minimizes $\psi_{ProxyDR}^2(s, \theta_c)$.

S2 Appendix

Dataset details.

All plankton images were obtained using FlowCam (Yokogawa Fluid Imaging Technologies). FlowCam is a flow imaging microscope that captures particles flowing through glass flowcells with well-defined volumes. The three plankton datasets were obtained according to different types of samples (live and Lugol fixed whole seawater or 180 μm WP2 plankton net samples) using three different FlowCams (FlowCam 8400, FlowCam VS, and FlowCam Macro) with various magnifications. Thus, the datasets include particles ranging from 5 to 2000 μm in size, thus representing nano-, micro-, and mesozooplankton. The plankton samples were obtained from three coastal monitoring stations (Institute of Marine Research) along the Norwegian coast, including Holmfjord in the north, Austevoll in the west and Torungen in the south. In addition, for the nano- and microplankton, seawater samples were obtained from a tidal zone at a depth of 1 meter at the research station at Flødevigen in southern Norway, which is approximately 2 nautical miles from the southern monitoring station at Torungen. The sampling period for the three datasets covered all seasons over a period of approximately 2.5 years.

Small microplankton (MicroS) This dataset contains images of fixed and live seawater samples acquired at a depth of 5 m at the three monitoring stations and a depth of 1 m in the tidal zone (see above). The seawater samples were carefully filtered through a 80 μm mesh to ensure that 100 μm flowcell was not clogged and imaged using a 10 \times objective. This FlowCam configuration results in a total magnification of 100 \times and images particles ranging from 5 to 50 μm . Before resizing, one pixel in an image represented 0.7330 μm .

Large microplankton (MicroL) This dataset contains images of fixed and live seawater samples acquired at a depth of 5 m at the three monitoring stations and a depth of 1 m in the tidal zone (see above). The seawater samples were not filtered and were imaged using a 2 \times objective, targeting 35 to 500 μm particles. Before resizing, one pixel in an image represented 2.9730 μm . Due to instrument repair and adjustments to improve image quality, the camera settings were modified during the 3 years of imaging to acquire this dataset. Therefore, the image appearance and quality are slightly variable.

Mesozooplankton (MesoZ) This dataset contains images of mesozooplankton samples acquired at the three coastal monitoring stations (see above) and a transect in the Norwegian Sea (Svinøysnippet). The samples were obtained using an IMR (Institute of Marine Research) standard plankton net (WP2) or a multinet mammoth (both 180 μm mesh) and fixed with 4% formaldehyde. The images were acquired by two FlowCam instruments (one in Bergen and one in Flødevigen), and the image appearance differs slightly between the two instruments. The FlowCam macro was equipped with a 0.5 \times objective, resulting in a total magnification of 12.5 and imaging organisms ranging from 180 to 2000 μm . Before resizing, one pixel in an image represented 9.05 μm . All images in the mesozooplankton dataset are in grayscale.

NABirds Data provided by the Cornell Lab of Ornithology, with thanks to photographers and contributors of crowdsourced data at AllAboutBirds.org/Labs. This material is based upon work supported by the National Science Foundation under Grant No. 1010818.

Hierarchical structures of the datasets Figs. S1, S2, and S3 and Table S1 show the hierarchical structures of the datasets. As the NABirds dataset contains too many (555) classes to visualize, we do not show the hierarchical structures of the NABirds dataset [27]. We used the hierarchy provided by the Cornell Lab of Ornithology.

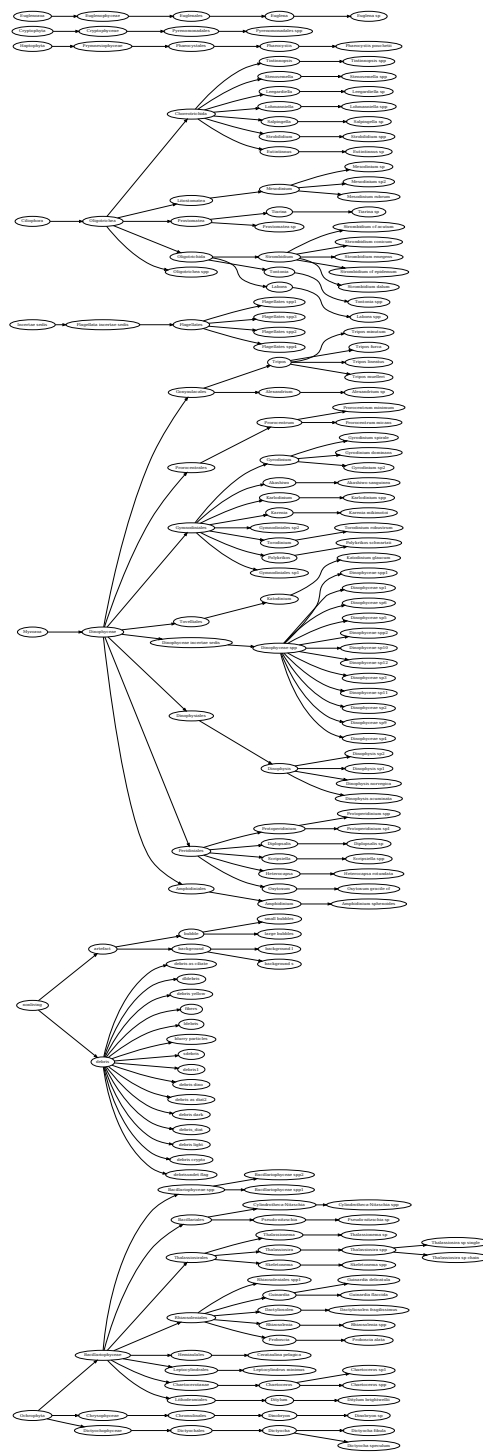


Fig S1. The hierarchical structure of the MicroS dataset used in our experiment. Best viewed by zooming in.

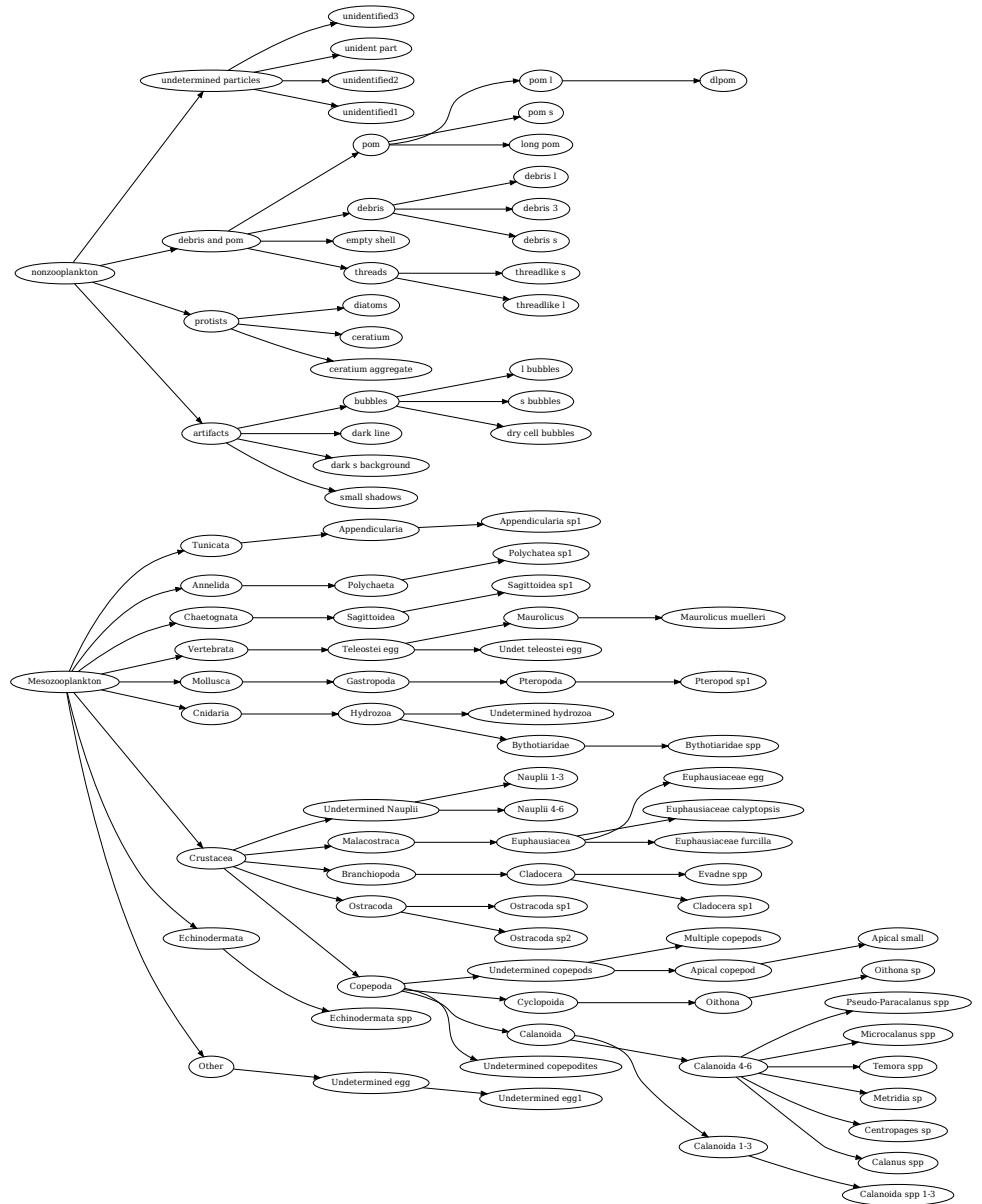


Fig S3. The hierarchical structure of the MesoZ dataset used in our experiment. Best viewed by zooming in.

Table S1. The hierarchical structure of the CIFAR100 dataset used in our experiment.

Level 0	Level 1	Level 2	Level 3 (class level)
Animals	Invertebrates	insects	bee, beetle, butterfly, caterpillar, cockroach
		non-insect invertebrates	crab, lobster, snail, spider, worm
	Mammals	aquatic mammals	beaver, dolphin, otter, seal, whale
		large carnivores	bear, leopard, lion, tiger, wolf
		large omnivores and herbivores	camel, cattle, chimpanzee, elephant, kangaroo
		medium-sized mammals	fox, porcupine, possum, raccoon, skunk
		people	baby, boy, girl, man, woman
		small mammals	hamster, mouse, rabbit, shrew, squirrel
	Non-mammal vertebrates	fish	aquarium fish, flatfish, ray, shark, trout
		reptiles	crocodile, dinosaur, lizard, snake, turtle
Artificial	Artificial (indoor)	food containers	bottles, bowls, cans, cups, plates
		household electrical devices	clock, computer keyboard, lamp, telephone, television
		household furniture	bed, chair, couch, table, wardrobe
	Artificial (outdoor)	large man-made outdoor things	bridge, castle, house, road, skyscraper
		vehicles 1	bicycle, bus, motorcycle, pickup truck, train
		vehicles 2	lawn-mower, rocket, streetcar, tank, tractor
Nature (non-animal)	Nature (non-specific organism)	large natural outdoor scenes	cloud, forest, mountain, plain, sea
	Plants	flowers	orchids, poppies, roses, sunflowers, tulips
		fruit and vegetables	apples, mushrooms, oranges, pears, sweet peppers
		trees	maple, oak, palm, pine, willow

S3 Appendix

Results for all five datasets.

Figs. S4, S5, S6, S7, and S8 show the top- k accuracies on the different datasets.

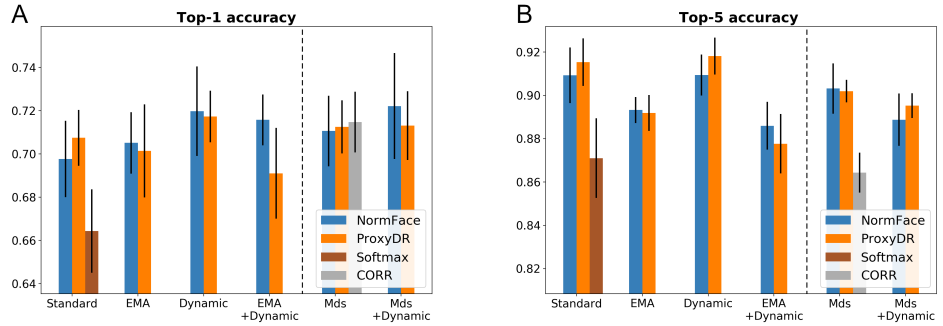


Fig S4. Top- k accuracy results (A: $k = 1$, B: $k = 5$) on the MicroS dataset.

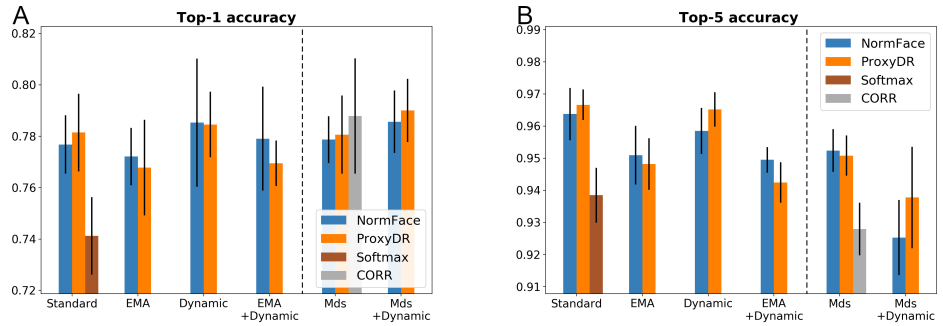


Fig S5. Top- k accuracy results (A: $k = 1$, B: $k = 5$) on the MicroL dataset.

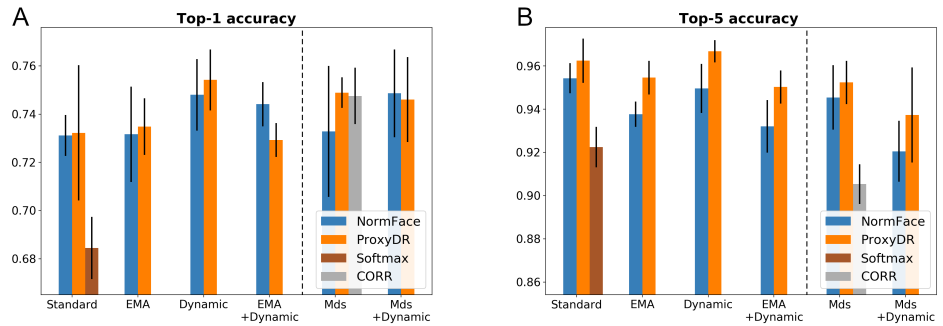


Fig S6. Top- k accuracy results (A: $k = 1$, B: $k = 5$) on the MesoZ dataset.

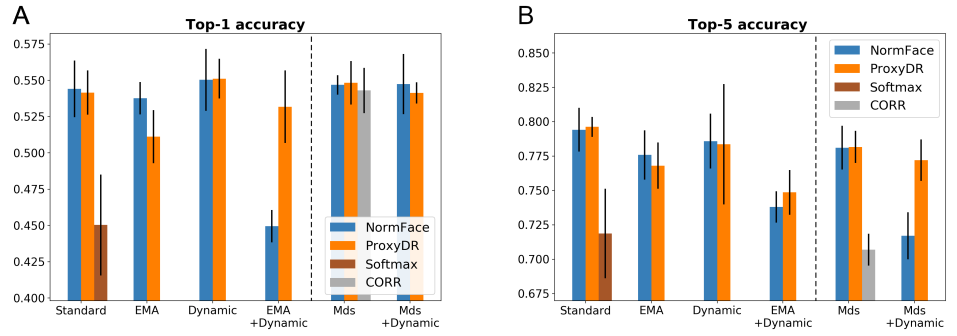


Fig S7. Top- k accuracy results (A: $k = 1$, B: $k = 5$) on the CIFAR100 dataset.

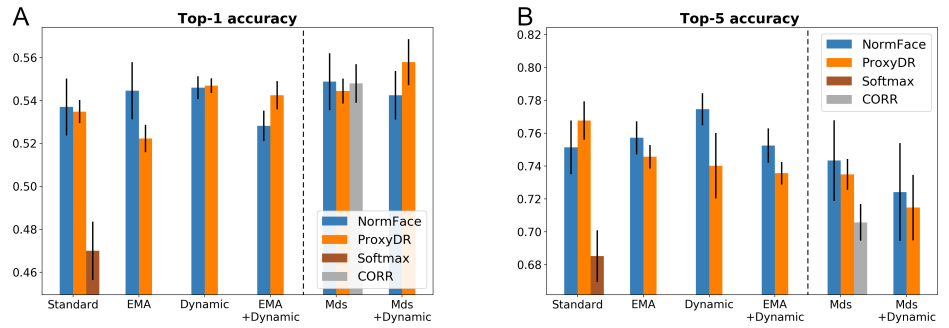


Fig S8. Top- k accuracy results (A: $k = 1$, B: $k = 5$) on the NABirds dataset.

Figs. S9, S10, S11, S12, and S13 show the mean correlation values on the different datasets.

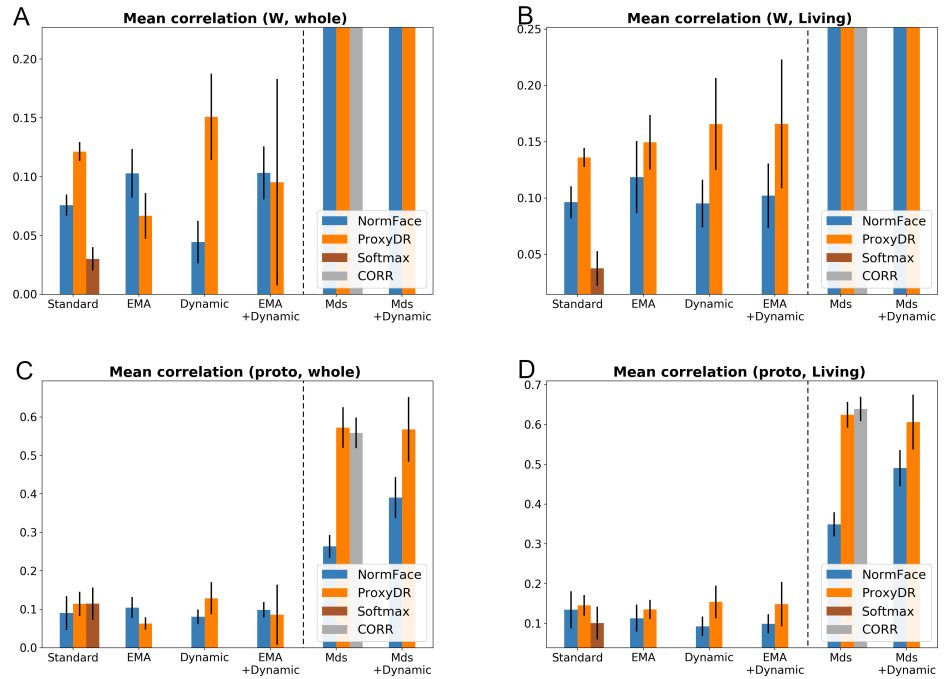


Fig S9. Correlation measures on the MicroS dataset. (Top) Values using proxies (A: whole classes, B: living classes). (Bottom) Values using prototypes (C: whole classes, D: living classes). ‘Living’ indicates that only biological classes were used (no nonliving classes). The mean correlation values based on proxies with the MDS option were 0.9306 (whole) and 0.9011 (living).

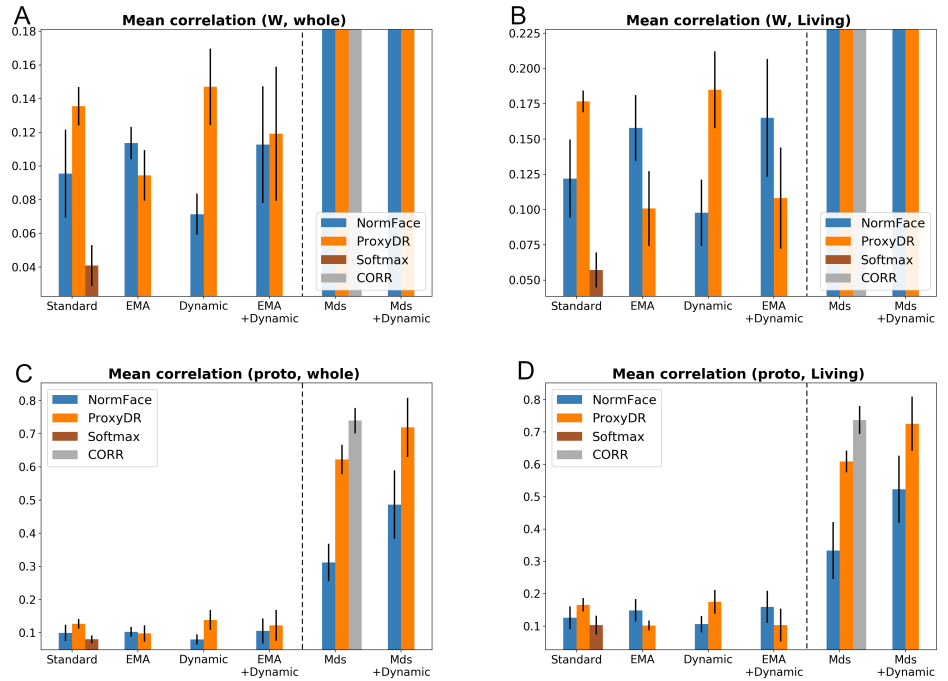


Fig S10. Correlation measures on the MicroL dataset. (Top) Values using proxies (A: whole classes, B: living classes). (Bottom) Values using prototypes (C: whole classes, D: living classes). The mean correlation values based on proxies with the MDS option were 0.9543 (whole) and 0.9426 (living).

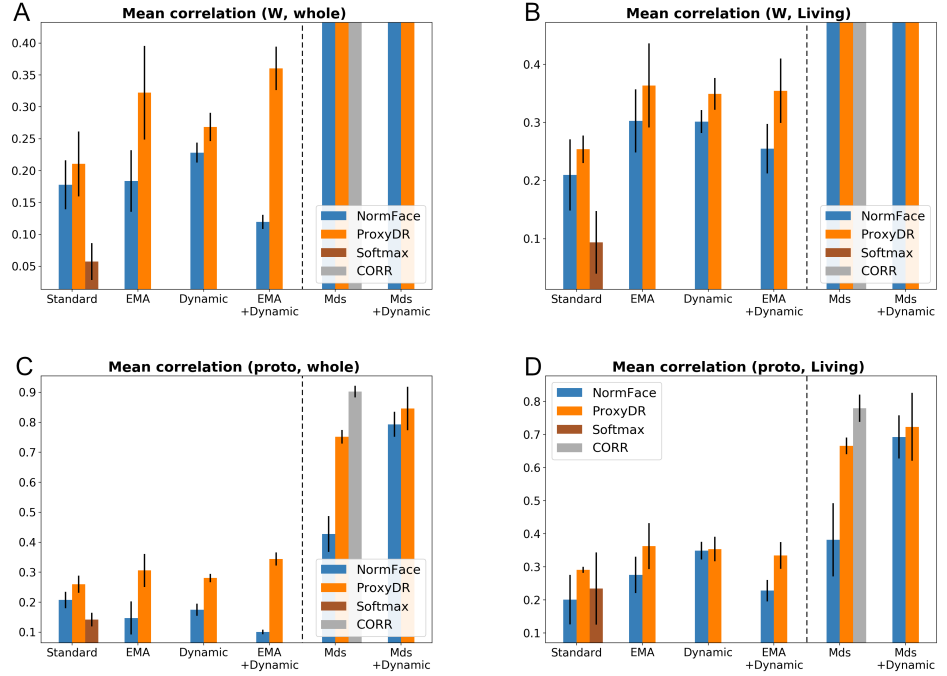


Fig S11. Correlation measures on the MesoZ dataset. (Top) Values using proxies (A: whole classes, B: living classes). (Bottom) Values using prototypes (C: whole classes, D: living classes). The mean correlation values based on proxies with the MDS option were 0.9783 (whole) and 0.9602 (living).

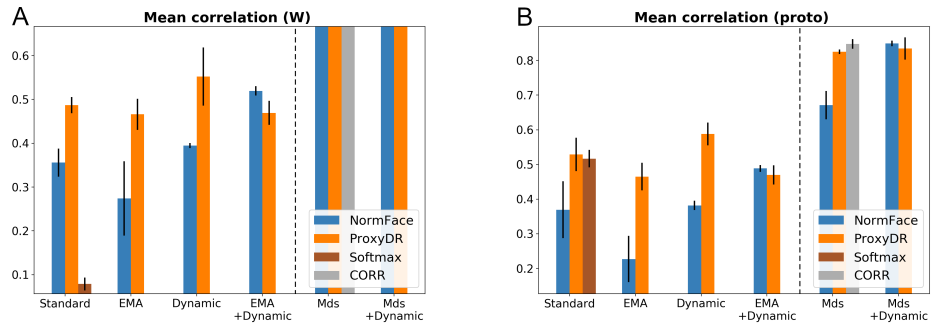


Fig S12. Correlation measures on the CIFAR100 dataset. (A) Values using proxies. (B) Values using prototypes. The mean correlation value based on proxies with the MDS option was 0.8580.

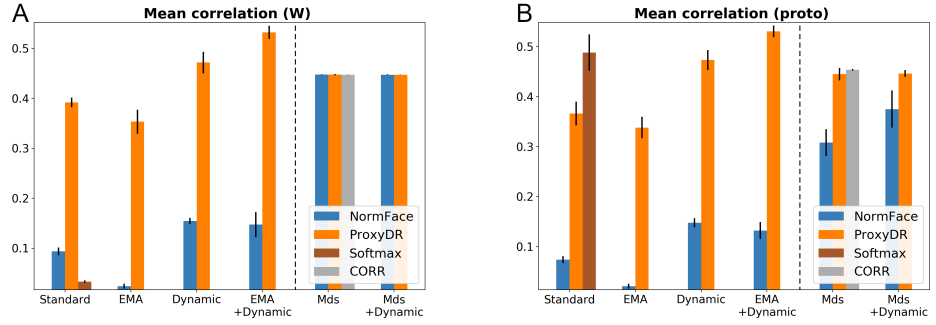


Fig S13. Correlation measures on the NABirds dataset. (A) Values using proxies. (B) Values using prototypes. The mean correlation value based on proxies with the MDS option was 0.4476 (this value is small as the dataset contains 555 classes and the embedding dimension is 128).

Figs. S14, S15, S16, S17, and S18 show the hierarchy-informed performance measures on the different datasets.

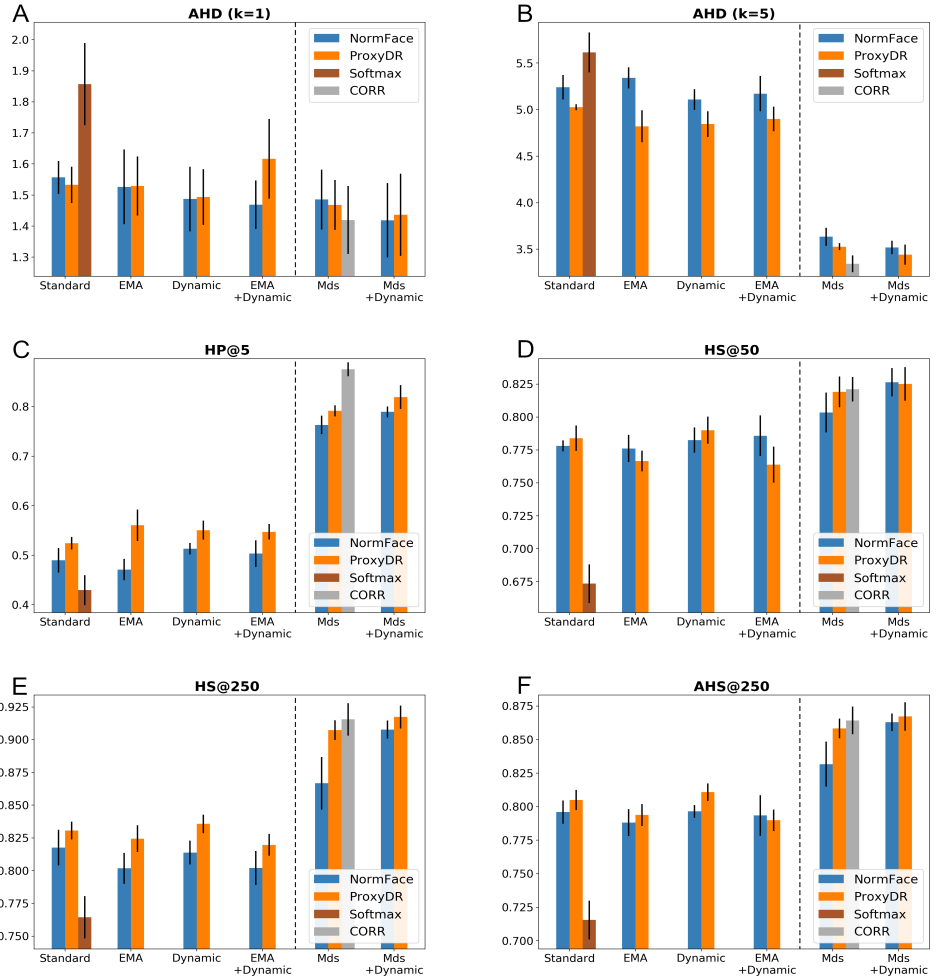


Fig S14. Hierarchical performance measures on the MicroS dataset. The symbol \downarrow denotes that lower values indicate better performance. The symbol \uparrow denotes that higher values indicate better performance. (A) AHD ($k=1$): \downarrow . (B) AHD ($k=5$): \downarrow . (C) HP@5: \uparrow . (D) HS@50: \uparrow . (E) HS@250: \uparrow . (F) AHS@250: \uparrow .

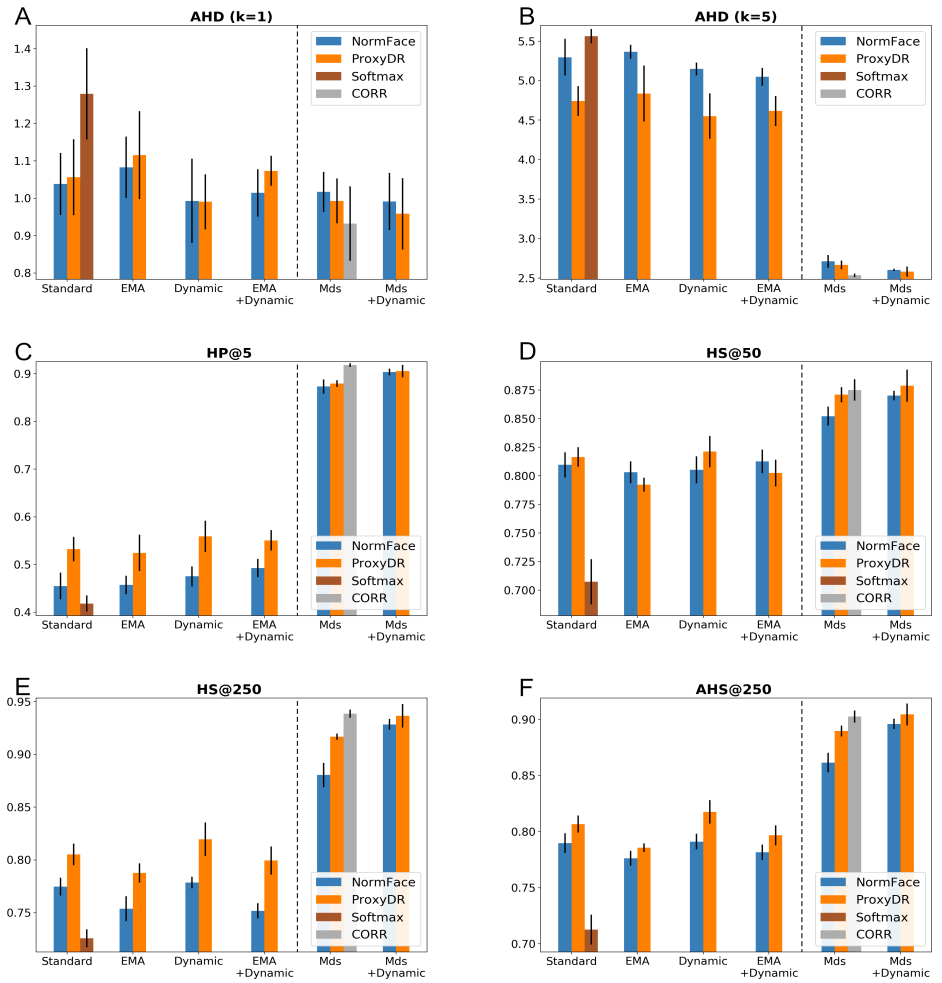


Fig S15. Hierarchical performance measures on the MicroL dataset. The symbol \downarrow denotes that lower values indicate better performance. The symbol \uparrow denotes that higher values indicate better performance. (A) AHD (k=1): \downarrow . (B) AHD (k=5): \downarrow . (C) HP@5: \uparrow . (D) HS@50: \uparrow . (E) HS@250: \uparrow . (F) AHS@250: \uparrow .

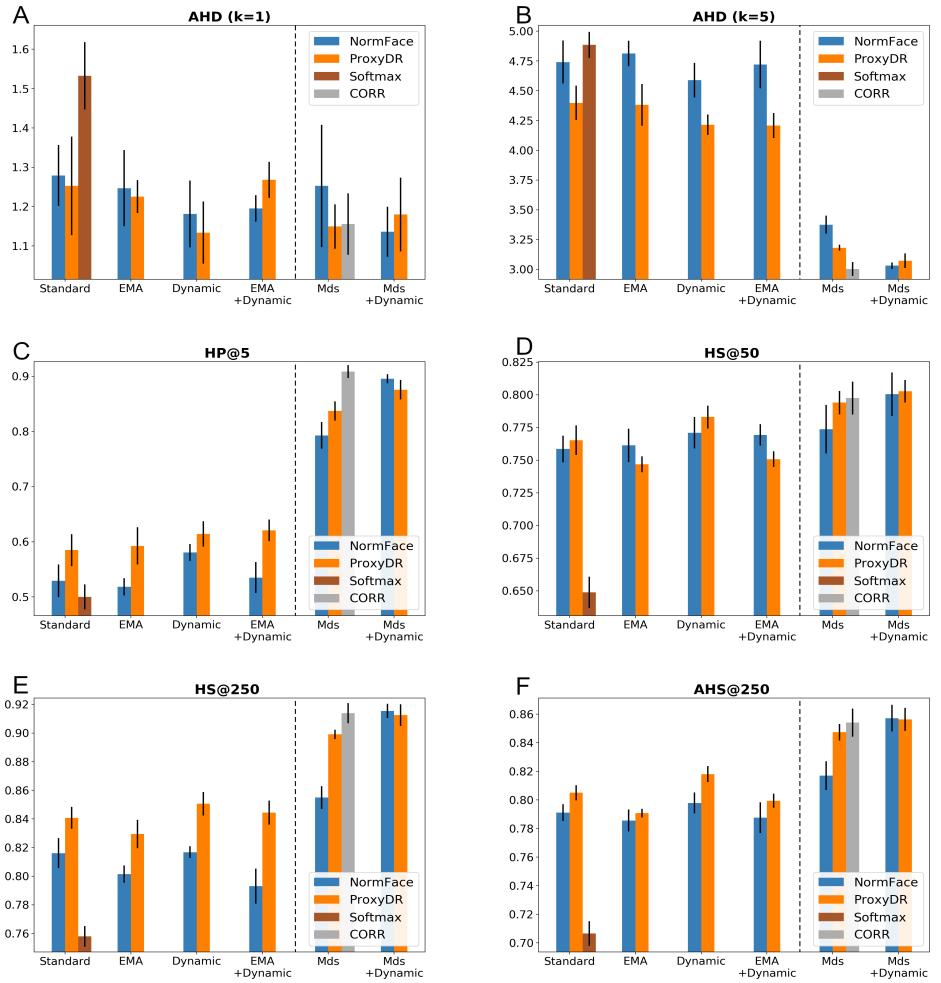


Fig S16. Hierarchical performance measures on the MesoZ dataset. The symbol \downarrow denotes that lower values indicate better performance. The symbol \uparrow denotes that higher values indicate better performance. (A) AHD (k=1): \downarrow . (B) AHD (k=5): \downarrow . (C) HP@5: \uparrow . (D) HS@50: \uparrow . (E) HS@250: \uparrow . (F) AHS@250: \uparrow .

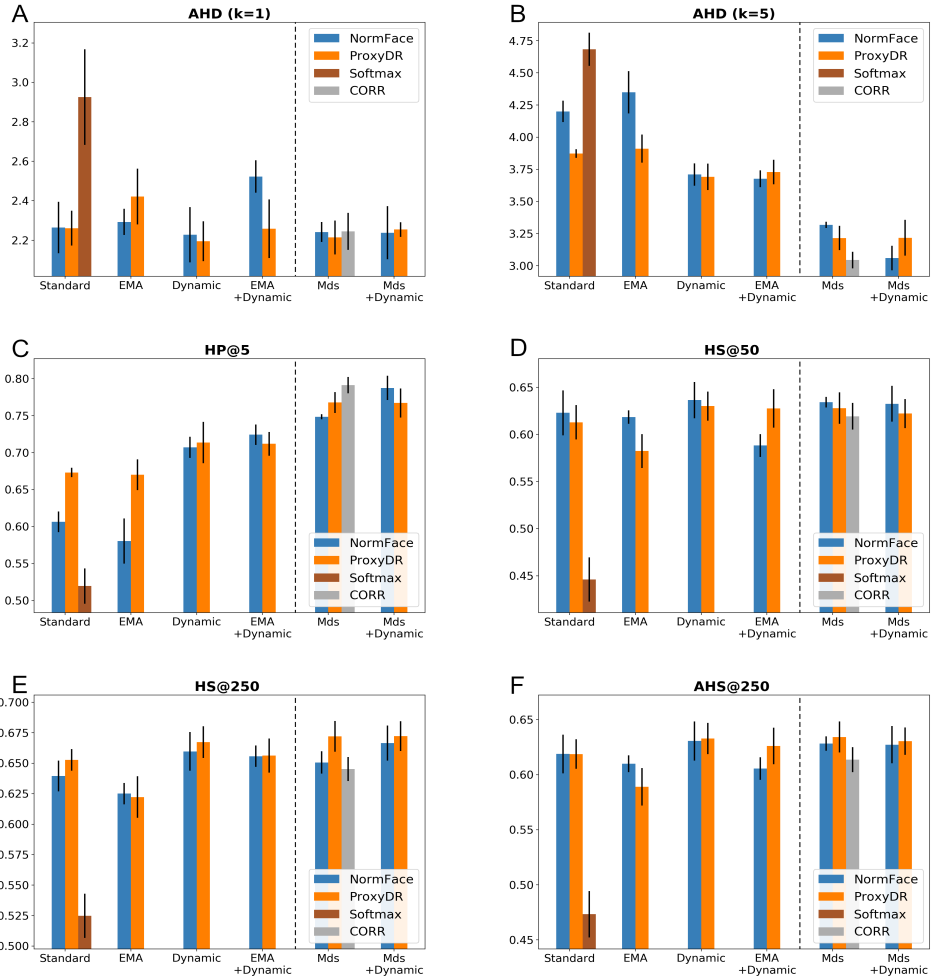


Fig S17. Hierarchical performance measures on the CIFAR100 dataset. The symbol \downarrow denotes that lower values indicate better performance. The symbol \uparrow denotes that higher values indicate better performance. (A) AHD (k=1): \downarrow . (B) AHD (k=5): \downarrow . (C) HP@5: \uparrow . (D) HS@50: \uparrow . (E) HS@250: \uparrow . (F) AHS@250: \uparrow .

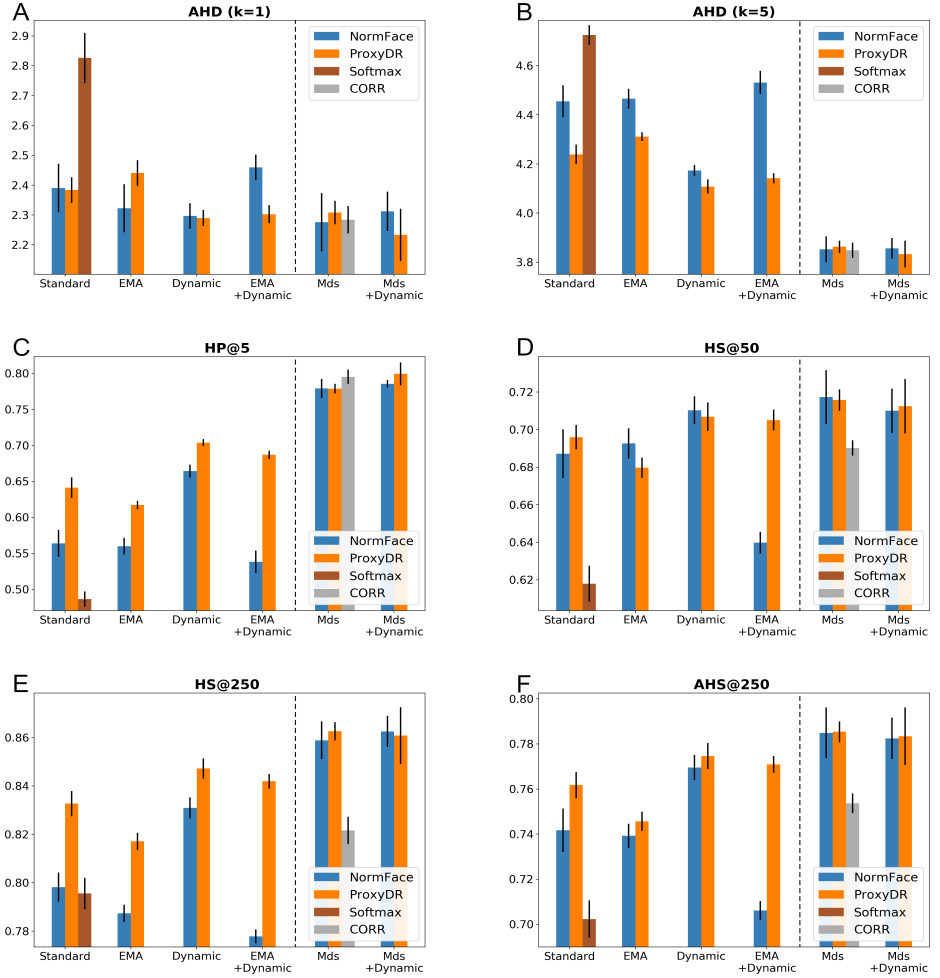


Fig S18. Hierarchical performance measures on the NABirds dataset. The symbol \downarrow denotes that lower values indicate better performance. The symbol \uparrow denotes that higher values indicate better performance. (A) AHD ($k=1$): \downarrow . (B) AHD ($k=5$): \downarrow . (C) HP@5: \uparrow . (D) HS@50: \uparrow . (E) HS@250: \uparrow . (F) AHS@250: \uparrow .

Additional results on mean correlations

Figs. S19, S20, S21, S22, S23 and S24 visualize the changes in the mean correlation values with different models and training options, showing the averaged values for five different seeds. Figs. S19 and S22 show that the accuracy of the NormFace models decreased after a certain number of epochs when the models were trained with the dynamic option. Interestingly, the mean correlation values increased even when the accuracy decreased. When using predefined hierarchical information and dynamic options (if applicable), the prototype-based mean correlation values approached the fixed proxy-based mean correlation values, except the NormFace model on the NABirds dataset.

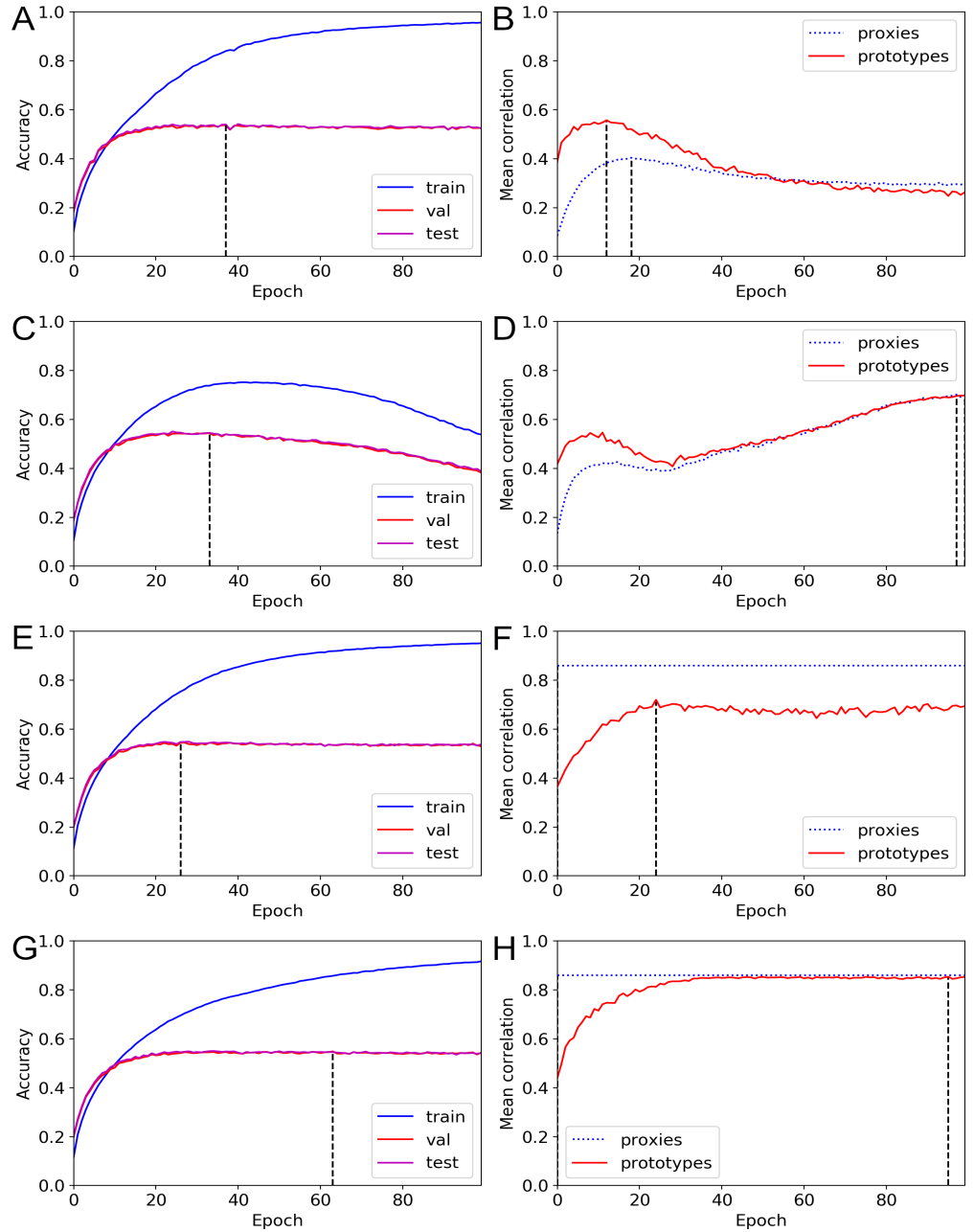


Fig S19. Changes in accuracy and mean correlations for the CIFAR100 dataset (NormFace). (A) Accuracy curve with standard training. (B) Mean correlation curve with standard training. (C) Accuracy curve with the dynamic option. (D) Mean correlation curve with the dynamic option. (E) Accuracy curve with the MDS option. (F) Mean correlation curve with the MDS option. (G) Accuracy curve with the MDS & dynamic options. (H) Mean correlation curve with the MDS & dynamic options.

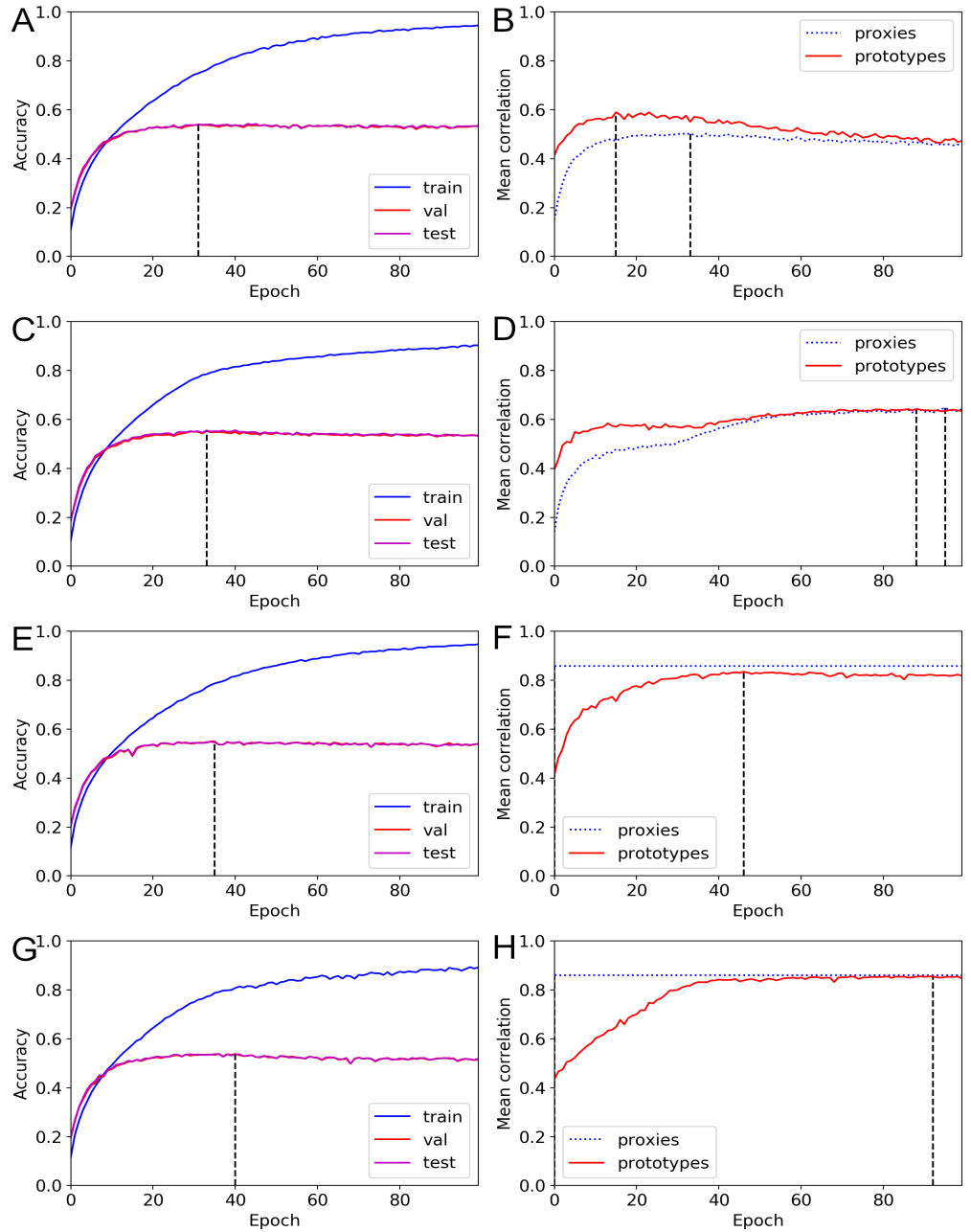


Fig S20. Changes in accuracy and mean correlations for the CIFAR100 dataset (ProxyDR). (A) Accuracy curve with standard training. (B) Mean correlation curve with standard training. (C) Accuracy curve with the dynamic option. (D) Mean correlation curve with the dynamic option. (E) Accuracy curve with the MDS option. (F) Mean correlation curve with the MDS option. (G) Accuracy curve with the MDS & dynamic options. (H) Mean correlation curve with the MDS & dynamic options.

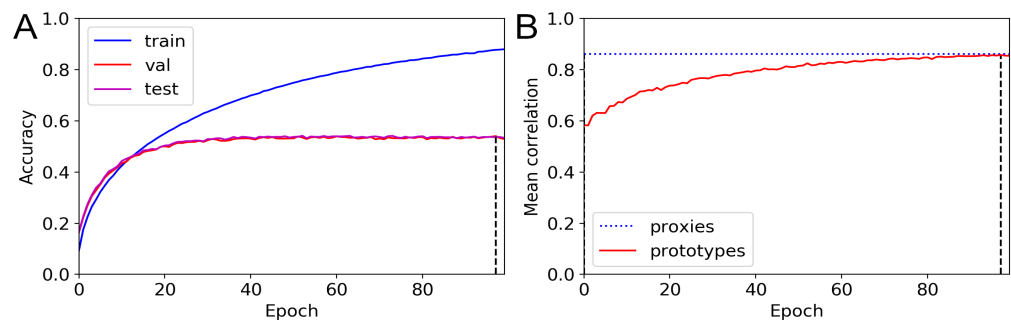


Fig S21. Changes in accuracy and mean correlations for the CIFAR100 dataset (CORR). (A) Accuracy curve with CORR loss training. (B) Mean correlation curve with CORR loss training.

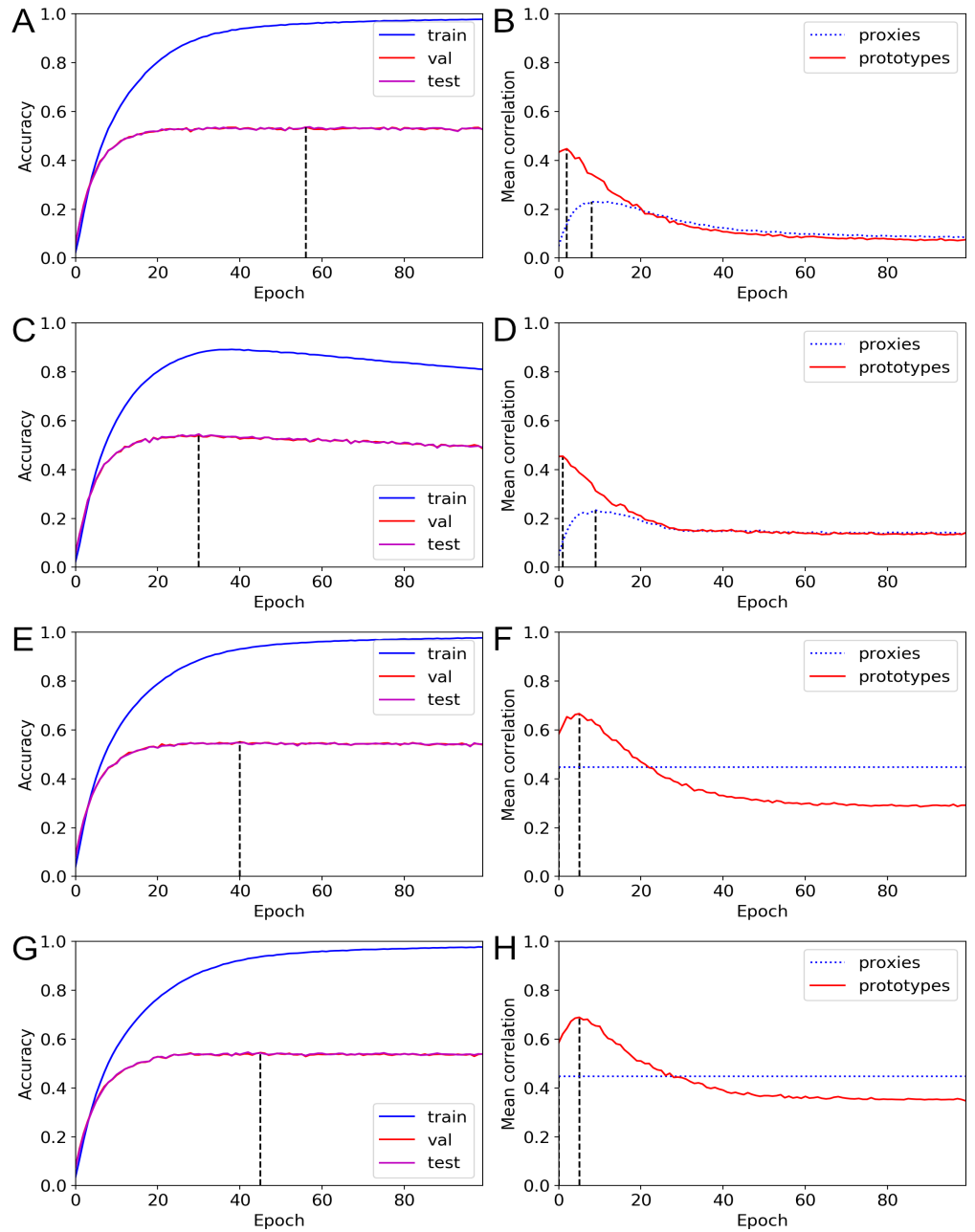


Fig S22. Changes in accuracy and mean correlations for the NABirds dataset (NormFace). (A) Accuracy curve with standard training. (B) Mean correlation curve with standard training. (C) Accuracy curve with the dynamic option. (D) Mean correlation curve with the dynamic option. (E) Accuracy curve with the MDS option. (F) Mean correlation curve with the MDS option. (G) Accuracy curve with the MDS & dynamic options. (H) Mean correlation curve with the MDS & dynamic options.

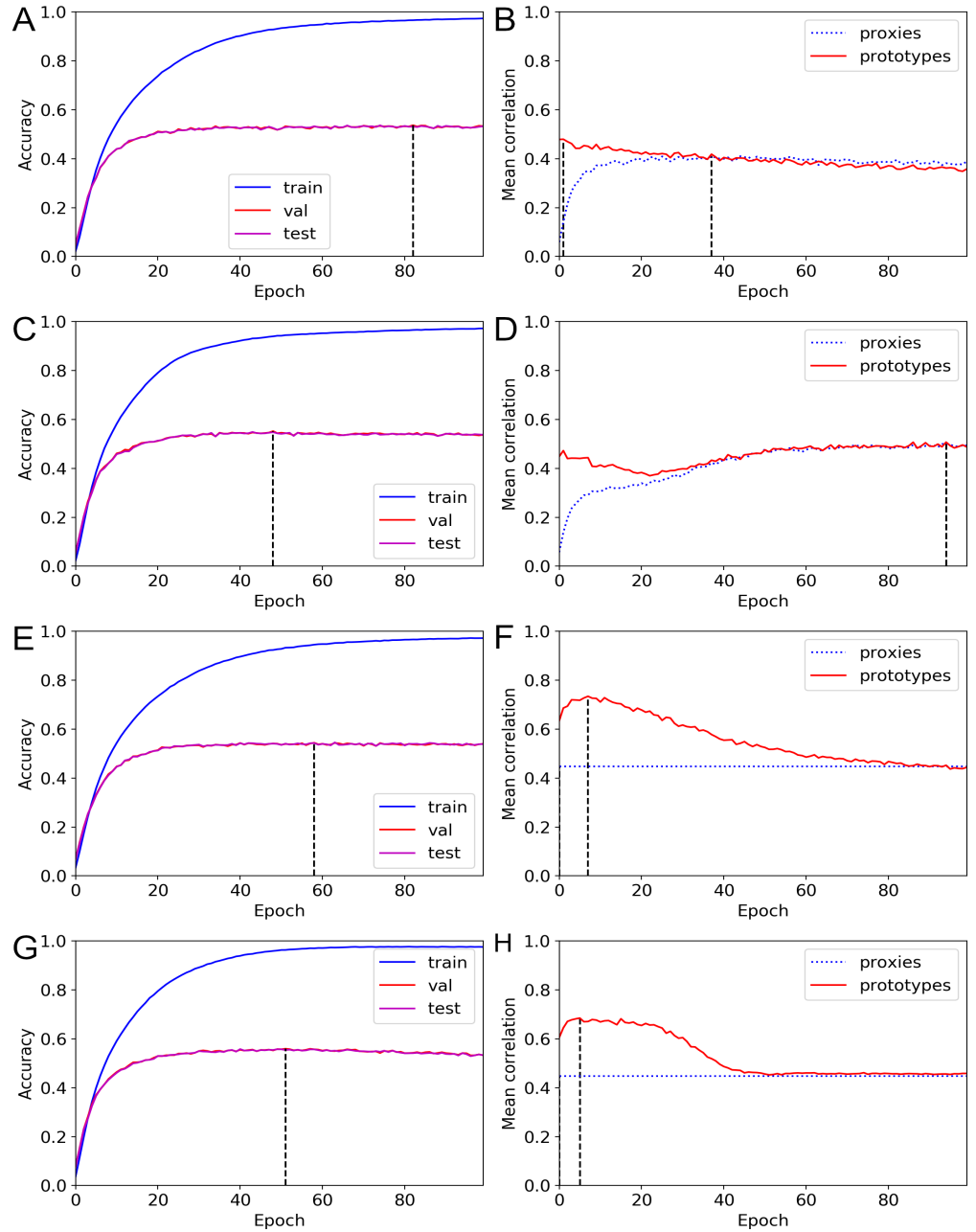


Fig S23. Changes in accuracy and mean correlations for the NABirds dataset (ProxyDR). (A) Accuracy curve with standard training. (B) Mean correlation curve with standard training. (C) Accuracy curve with the dynamic option. (D) Mean correlation curve with the dynamic option. (E) Accuracy curve with the MDS option. (F) Mean correlation curve with the MDS option. (G) Accuracy curve with the MDS & dynamic options. (H) Mean correlation curve with the MDS & dynamic options.

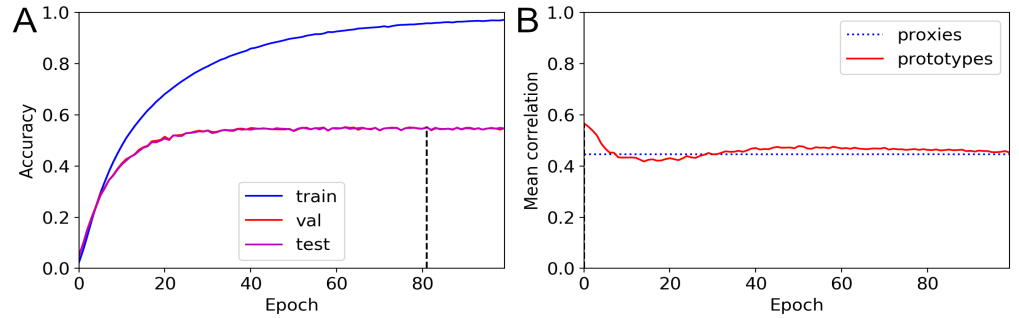


Fig S24. Changes in accuracy and mean correlations for the NABirds dataset (CORR). (A) Accuracy curve with CORR loss training. (B) Mean correlation curve with CORR loss training.

Rank correlations between performance measures We investigate whether different performance measures are correlated. While we cannot derive causal relationships, this investigation is useful for determining if there are trade-offs between various performance measures. We used rank correlation coefficients between the mean correlation values and other measures. We ignored the softmax loss results, as this model is not based on metric learning.

In Table S2, we investigate whether mean correlation values based on proxies (Figs. S9, S10, S11, S12, and S13) are correlated with other performance measures (Figs. S4, S5, S6, S7, S8, S14, S15, S16, S17, and S18). The table shows that the AHD ($k=5$), HP@5, HS@250, and AHS@250 measures are correlated with the proxy-based mean correlation values. Moreover, there does not appear to be any trade-off between the top-1 accuracies and proxy-based mean correlations. However, a trade-off between the top-5 accuracy and proxy-based mean correlations is observed on some datasets.

Table S2. Rank (Spearman) correlation coefficients of different measures with mean correlations (based on proxies)

Measure	MicroS	MicroL	MesoZ	CIFAR100	NABirds
Top-1	0.2039 (1.0336×10^{-1})	0.2260 (7.0284×10^{-2})	0.2171 (8.2377×10^{-2})	0.1675 (1.8239×10^{-1})	0.3112 (1.1627×10^{-2})
Top-5	-0.1350 (2.8361×10^{-1})	-0.3716 (2.3043×10^{-3})	-0.2120 (9.0045×10^{-2})	-0.3364 (6.1476×10^{-3})	-0.5669 (8.4964×10^{-7})
AHD (k=1)	-0.3423 (5.2583×10^{-3})	-0.3855 (1.5179×10^{-3})	-0.2959 (1.6684×10^{-2})	-0.1821 (1.4658×10^{-1})	-0.4267 (3.9270×10^{-4})
AHD (k=5)	-0.7407 (1.7522×10^{-12})	-0.8258 (2.5540×10^{-17})	-0.9026 (9.6705×10^{-25})	-0.8856 (1.1648×10^{-22})	-0.7023 (7.0541×10^{-11})
HP@5	0.7392 (2.0489×10^{-12})	0.8350 (5.4193×10^{-18})	0.9001 (2.0612×10^{-24})	0.8955 (7.8000×10^{-24})	0.7070 (4.6412×10^{-11})
HS@50	0.7671 (9.2047×10^{-14})	0.7962 (2.2284×10^{-15})	0.5634 (1.0275×10^{-6})	0.1878 (1.3410×10^{-1})	0.5276 (6.3074×10^{-6})
HS@250	0.7911 (4.4738×10^{-15})	0.8167 (1.1029×10^{-16})	0.8860 (1.0514×10^{-22})	0.5514 (1.9333×10^{-6})	0.7210 (1.2570×10^{-11})
AHS@250	0.7950 (2.6376×10^{-15})	0.8186 (8.1611×10^{-17})	0.8034 (8.1089×10^{-16})	0.3335 (6.6355×10^{-3})	0.6862 (2.8150×10^{-10})

p values are written in parentheses. Significant results (p value < 0.01) are written in bold text.

In Table S3, we investigate whether the top-1 accuracy (Figs. S4, S5, S6, S7, and S8) is correlated with other performance measures (Figs. S4, S5, S6, S7, S8, S14, S15, S16, S17, and S18). The table shows that the AHD (k=1), HS@50, and AHS@250 measures are correlated with the top-1 accuracy. Note that these are the measures that did not show noticeable changes on some datasets when predefined hierarchical information was used during training.

Table S3. Rank (Spearman) correlation coefficients of different measures with the top-1 accuracy

Measure	MicroS	MicroL	MesoZ	CIFAR100	NABirds
Top-5	0.2199 (7.8357×10^{-2})	0.0365 (7.7302×10^{-1})	0.1033 (4.1302×10^{-1})	0.4398 (2.4659×10^{-4})	-0.1043 (4.0815×10^{-1})
AHD (k=1)	-0.8005 (1.2168×10^{-15})	-0.8302 (1.2369×10^{-17})	-0.9309 (2.9921×10^{-29})	-0.9507 (9.4257×10^{-34})	-0.9509 (8.6632×10^{-34})
AHD (k=5)	-0.1906 (1.2829×10^{-1})	-0.3259 (8.0758×10^{-3})	-0.2908 (1.8752×10^{-2})	-0.2877 (2.0115×10^{-2})	-0.6136 (5.4992×10^{-8})
HP@5	0.2263 (6.9923×10^{-2})	0.2956 (1.6811×10^{-2})	0.2886 (1.9712×10^{-2})	0.2439 (5.0222×10^{-2})	0.6029 (1.0692×10^{-7})
HS@50	0.4325 (3.2041×10^{-4})	0.5085 (1.5301×10^{-5})	0.6979 (1.0420×10^{-10})	0.8967 (5.5302×10^{-24})	0.6832 (3.6174×10^{-10})
HS@250	0.1369 (2.7674×10^{-1})	0.3057 (1.3279×10^{-2})	0.2945 (1.7269×10^{-2})	0.5535 (1.7312×10^{-6})	0.4915 (3.2203×10^{-5})
AHS@250	0.3394 (5.6730×10^{-3})	0.4233 (4.4195×10^{-4})	0.5067 (1.6583×10^{-5})	0.8517 (2.4413×10^{-19})	0.5733 (6.0057×10^{-7})
Mean correlation (proxy)	0.2039 (1.0336×10^{-1})	0.2260 (7.0284×10^{-2})	0.2171 (8.2377×10^{-2})	0.1675 (1.8239×10^{-1})	0.3112 (1.1627×10^{-2})
Mean correlation (prototype)	0.2150 (8.5503×10^{-2})	0.2055 (1.0051×10^{-1})	0.1738 (1.6616×10^{-1})	0.1978 (1.1423×10^{-1})	0.2664 (3.1936×10^{-2})

p values are written in parentheses. Significant results (p value < 0.01) are written in bold text.

In Table S4, we investigate whether the top-5 accuracy (Figs. S4, S5, S6, S7, and S8) is correlated with other performance measures (Figs. S4, S5, S6, S7, S8, S14, S15, S16, S17, and S18). The table shows that no measures are correlated with the top-5 accuracy on all datasets.

Table S4. Rank (Spearman) correlation coefficients of different measures with the top-5 accuracy

Measure	MicroS	MicroL	MesoZ	CIFAR100	NABirds
Top-1	0.2199 (7.8357×10^{-2})	0.0365 (7.7302×10^{-1})	0.1033 (4.1302×10^{-1})	0.4398 (2.4659×10^{-4})	-0.1043 (4.0815×10^{-1})
AHD (k=1)	-0.0716 (5.7106×10^{-1})	0.0033 (9.7911×10^{-1})	-0.0406 (7.4809×10^{-1})	-0.4245 (4.2428×10^{-4})	0.1196 (3.4268×10^{-1})
AHD (k=5)	0.2417 (5.2436×10^{-2})	0.4842 (4.3828×10^{-5})	0.2732 (2.7654×10^{-2})	0.4561 (1.3422×10^{-4})	0.4949 (2.7791×10^{-5})
HP@5	-0.2765 (2.5757×10^{-2})	-0.5318 (5.1600×10^{-6})	-0.3113 (1.1590×10^{-2})	-0.4902 (3.3964×10^{-5})	-0.5733 (5.9953×10^{-7})
HS@50	0.0115 (9.2784×10^{-1})	-0.3164 (1.0231×10^{-2})	-0.2331 (6.1677×10^{-2})	0.2515 (4.3295×10^{-2})	-0.0071 (9.5522×10^{-1})
HS@250	-0.0677 (5.9231×10^{-1})	-0.4343 (3.0034×10^{-4})	-0.1965 (1.1677×10^{-1})	0.0955 (4.4900×10^{-1})	-0.3192 (9.5513×10^{-3})
AHS@250	0.0249 (8.4393×10^{-1})	-0.3603 (3.1949×10^{-3})	-0.1446 (2.5059×10^{-1})	0.3157 (1.0404×10^{-2})	-0.2203 (7.7867×10^{-2})
Mean correlation (proxy)	-0.1350 (2.8361×10^{-1})	-0.3716 (2.3043×10^{-3})	-0.2120 (9.0045×10^{-2})	-0.3364 (6.1476×10^{-3})	-0.5669 (8.4964×10^{-7})
Mean correlation (prototype)	-0.1040 (4.0985×10^{-1})	-0.4784 (5.5679×10^{-5})	-0.2910 (1.8677×10^{-2})	-0.3675 (2.5967×10^{-3})	-0.5457 (2.5927×10^{-6})

p values are written in parentheses. Significant results (p value < 0.01) are written in bold text.